Comments to the Author:

Comment 1. Based on the reviews, I recommend this paper be accepted for publication in TC after minor revisions. In addition to addressing the reviewer comments, I have a few suggestions to improve the readability of the paper:

Authors. Thank you so much for your constructive comments. We have revised the manuscript accordingly with reference to your comments, two anonymous reviewers, and public review.

Comment 2. I strongly discourage the extensive use of supplemental material in this case. Supplemental material is best used for material that cannot be put in the main paper (e.g. multimedia) or technical details. As your supplemental figures are relevant to the main results and discussion, the readability of the paper would be improved if this material was included in the main paper instead. This will make your paper more accessible to readers.

Authors. As per the suggestion, one of the important figure (Supplementary Fig. S4) much relevant to the main result is now moved into the main text as Fig. 5 of the revised manuscript.

Comment 3. Line 85-95 and table 1: What in-situ data are you validating against? This needs to be described and referenced.

Authors. This is included in the revised manuscript. The pixel values from the models were extracted around each in-situ observations of NPP to generate the matchups for the validation strategy. The details of in-situ measurement (^{13}C method) is documented in the previous work (Gandhi et al., 2012).

Comment 4. Materials and Methods – here you list what data you use, but it's not clear in what way it is used. E.g. the Argo float data, and eddy data. This section could be improved if you simply state how each of these data sets will be used.

Authors. This section is improved in the revised manuscript by including how the datasets are being used.

Comment 5. Line 142 – "missing" might imply you had no data, but I think you mean that no chl-a was observed.

Authors. Modified the sentence as 'no chl-a wa observed' in place of 'missing'.

Comment 6. Line 157 – If it's only one float, it's not a fleet.

Authors. Removed the word 'fleet of' in the revised manuscript.

Comment 7. Figure S9 – please be clear if this is incident shortwave or absorbed shortwave. Also, please indicate where this data is from in the revised manuscript.

Authors. Yes, this is an incident shortwave radiation which has been specified in the revised manuscript. The revised figure number is now Figure-S6. The monthly incident shortwave radiation was acquired from the European Center for Medium-Range Weather Forecast (ECMWF) at grid resolution of 0.25° during January 1979-December 2017. Monthly anomalies of shortwave radiation for September-November 2017 was computed relative to a 38-year climatology (1979-2016). The details are incorporated in the revised text.

Comment 8. Figure S6 – specify which is Weddell Sea polynya and which is Maud Rise Polynya.

Authors. The figure is revised as per the suggestion. Reappearance of the Weddell Sea polynya is shown within the red rectangles and Maud Rise as black rectangles. The revised figure number is now Figure-S8.

Comment 9. Non-public comments to the Author:

There is numerous instances of awkward English phrasing and syntax throughout the manuscript that impacts the readability. If accepted, the manuscript will be copyedited before publication, but I recommend a careful reading through and editing to correct as many of these as possible now to ensure your intended meaning is clear.

Authors. We have tried to improve for the English phrasing so as to convey the intended meaning in the manuscript. Thank you so much for your suggestion that has indeed helped to improve the quality of the manuscript.

Satellite observations of ~~new~~ unprecedented phytoplankton blooms in the Maud Rise Polynya, Southern Ocean

Babula Jena, and Anilkumar Narayana Pillai

ESSO - National Centre for Polar and Ocean Research, Ministry of Earth Science, Government of India, Vasco-da-Gama, India.

Correspondence to: Babula Jena (bjena@ncpor.res.in)

Abstract. Appearance of new phytoplankton blooms with in the sea-ice cover has large importance considering the upper ocean primary production that controls the biological pump with the implications for atmospheric CO_2 and global climate. Satellite derived chlorophyll-*a* concentration showed the unprecedented phytoplankton blooms in the Maud Rise polynya, Southern Ocean with chlorophyll-*a* reached up to 4.67 mg m^{-3}. Multi-satellite data indicated that the bloom appeared for the first time in the entire mission records started since 1978. Argo float located in the polynya edge provided evidence of bloom condition in austral spring 2017 (chlorophyll-*a* up to 5.47 mg m^{-3}) compared to the preceding years of prevailed low chlorophyll-*a*. The occurrence of bloom was associated with the supply of nutrients into the upper ocean through the Ekman upwelling (driven by wind stress curl and cyclonic ocean eddies), and improved light condition up to 61.9 Einstein m^{-2} day^{-1}. The net primary production from the Aqua-Moderate Resolution Imaging Spectroradiometer ~~Aqua MODIS~~ chlorophyll-based algorithm showed that the Maud Rise polynya was as productive as the Antarctic coastal polynyas with the carbon fixation rates reached up to 415.08 mg C m^{-2} day^{-1}. The study demonstrates how the phytoplankton in the Southern Ocean (specifically over the shallow bathymetric region) would likely respond in the future under a warming climate condition and continued melting of Antarctic sea-ice since 2016.

1 Introduction

Antarctica sea-ice has moderately increased during the satellite era from 1979 to 2015, with the regional heterogeneity that comprises of both increasing and decreasing pattern in different sectors (Turner et al., 2017). However, anomalously record lowest sea-ice extent and area observed since three successive years from 2016 to 2018 with the maximum melting occurred in 2017, corresponding to the upper ocean warming of the Southern Ocean (Fig. S1). Amid the pronounced melting, the largest and most prolonged Maud Rise (MR) open ocean polynya since the 1970s reappeared on 14 September 2017 (~9.3 × 10^3 km^2) that expanded maximum on 1 December 2017 (~298.1 × 10^3 km^2) and existed for 79 days (Jena et al., 2019). Appearance of the polynyas plays an important role for the oceanic phytoplankton and primary production that controls the biological pump of the ocean (Arrigo and Dijken, 2003; Shadwick et al., 2017), apart from its importance for marine mammals and birds (Labrousse et al., 2018; Stirling, 1997), global heat-salt fluxes (Tamura et al., 2008), Antarctic bottom

water properties (Zanowski et al., 2015), and atmospheric circulation (Weijer et al., 2017). However, due to their spatial dimension, the polynyas are generally not represented well in the ~~large-scale~~large-scale climate models, limiting the capability of simulating and projecting polynya ~~-~~related biophysical changes under future climate change scenario (Li et al., 2016).

The Southern Ocean (SO) is known as the~~a~~ largest high-nutrient low-chlorophyll (HNLC) area of the global ocean. Since the past 50 years, the loss of ice shelves and glaciers retreat around the Antarctic Peninsula has increased at least 24,000 km^2 in surface area of new open water that was rapidly colonised by new phytoplankton blooms, with new benthic and marine zooplankton communities in the SO (Peck et al., 2010). In the background of HNLC, the occurrence of polynyas can enhance the chlorophyll-*a* (chl-*a*) concentration (a proxy for phytoplankton biomass) due to the increase in surface area of new open waters and growth season of the phytoplankton (Kahru et al., 2016). The bloom occurrence in the SO has been linked with the oceanographic features such as jet streams, meanders and mesoscale eddies, which can lead to increased iron and silicate supply by the ocean upwelling (Strass et al., 2002), thereby improving co-limitation of nutrient and light for phytoplankton growth (Hoppe et al., 2017) . Oceanic eddies have been found to regulate chl-*a* variability in the SO with higher (lower) values observed for the cyclonic (anticyclones) eddies (Kahru et al., 2007). The polynyas of the Amundsen and Ross Seas have high primary productivity that contribute to the SO carbon dioxide (CO_2) sink (Alderkamp et al., 2012; Arrigo et al., 2008a; Arrigo and Alderkamp, 2012; Yager et al., 2012). The primary productivity of these regions reaching up to 3 g C m^{-2} d^{-1}, roughly 10 folds more than the SO mean productivity (Arrigo and Dijken, 2003). The high productivity values in the polynya have been attributed to the supply of iron from the upwelling of iron rich deep water (Planquette et al., 2013), sediment diffusion or resuspension followed by upwelling (Ardelan et al., 2010), atmospheric inputs (Cassar et al., 2007; Wagener et al., 2008), melting of sea-ice (Lannuzel et al., 2010; van der Merwe et al., 2011), iceberg delivered glacial debris (Raiswell et al., 2008), and melting of ice-shelves (Pritchard et al., 2009; Wåhlin et al., 2010). The Amundsen polynya is one of the productive polynyas of the Antarctica with the satellite derived chl-*a* (2.2 mg m^{-3}) are 40% greater than the Ross Sea Polynya (1.5 mg m^{-3})(Schofield et al., 2015). Although the polynyas are believed as the sites of phytoplankton blooms in spring (Arrigo and Dijken, 2003) and acts as sinks of atmospheric CO_2 because of both physical-chemical processes and biological activity (Bates et al., 1998; Mu et al., 2014), very little is known about the MR polynya due to its rare appearance. In this paper, we report first evidence of occurrence of phytoplankton bloom in the MR polynya from satellite derived ocean color data and the Argo float. Further, the role of physical processes for the occurrence of bloom in the polynya is examined using relevant physical oceanographic data, followed by its likely implication for ocean-atmospheric exchange of CO_2.

2 Materials and Methods

In order to understand the impact of bathymetry on the phytoplankton biomass, t~~T~~he MR seamount was mapped using bathymetric raster data (21601 × 10801 pixels) from Earth Topography One Arc-Minute Global Relief Model, 2009

(ETOPO1) (www.ngdc.noaa.gov). The raster data were converted to polyline features with a contour interval of 500 m for showing the extent of the seamount (Fig. 1a). Level-3 monthly composite of satellite derived near-surface chl-*a* imageries were used from the Nimbus-7 Coastal Zone Colour Scanner (CZCS), Sea-viewing Wide Field-of-view Sensor (SeaWiFS), Aqua-Moderate Resolution Imaging Spectroradiometer (Aqua-MODIS), and Visible Infrared Imaging Radiometer Suite (VIIRS), as per the availability of data from 1978 to 2017 (Fig. 1b-e). Level-2 Aqua-MODIS ascending passes were processed (relatively cloud free data) to generate the high spatial resolution (~1 km) chl-*a* images during 25 October (14:45 hours UTC), 06 November (15:05 hours UTC) and 21 November 2017 (14:25 hours UTC) (Fig. 2). We used a standard chl-*a* retrieving algorithm that uses combination of both lower and higher range of chl-*a* retrieval as described in the Algorithm Theoretical Basis Document (ATBD) from the NASA Earth Observing System Project Science Office (https://oceancolor.gsfc.nasa.gov/atbd/chlor_a/). In this study, we have used the criteria of chl-*a* $\geq$ 0.8 mg m^{-3} (Fitch and Moore, 2007), for defining a phytoplankton bloom after considering the underestimation tendency of chl-*a* measurement from satellite observations over the Southern Ocean (Jena, 2017).

In order to analyze the Aqua-MODIS derived net primary production (NPP), we have validated three ocean-color based models such as the vertically generalized production model (VGPM), *Eppley*-VGPM, and carbon-based productivity model (CbPM) for selecting the best model for the study region. We evaluated the performance of these models by comparing with the in-situ NPP estimated using ^{13}C tracer during the Indian scientific expedition to the Southern Ocean in 2009. The locations of in-situ NPP observations during the austral summer (February to April 2009) are presented in figure S2a. The in-situ NPP from 11 observations range from about 85.04 to 923.83 mg C m^{-2} day^{-1}. The detail method of ^{13}C measurement was documented in the previous work (Gandhi et al., 2012). The VGPM was developed for estimation of NPP from chlorophyll accounting into temperature dependency of chlorophyll-specific photosynthetic efficiency (Behrenfeld and Falkowski, 1997b). The *Eppley*-VGPM makes use of an exponential function developed from changes in growth rates of phytoplankton over varied temperature ranges for a wide variety of species (Eppley, Richard, 1972). Further, a new CbPM model was developed that uses the backscattering coefficients and chlorophyll-to-carbon ratios for estimation of phytoplankton carbon biomass and phytoplankton growth rates, respectively (Westberry et al., 2008). The model based NPP values were available in weekly time scale with a spatial resolution of ~4 km. The pixel values from the models were extracted around each in-situ observations of NPP to generate the matchups for the validation strategy, a method adopted by several authors (Jena, 2017; Johnson et al., 2013). The comparative statistical analysis suggested that the scatters were much better in the case of *Eppley*-VGPM estimated NPP (Fig. S2c) than those in the case of VGPM (Fig. S2b) and CbPM (Fig. S2d). A bias of -26.21 mg C m^{-2} day^{-1} for *Eppley*-VGPM obtained NPP value was much better than those obtained from the VGPM (bias = 104.40 mg C m^{-2} day^{-1}) and CbPM (bias = 94.14 mg C m^{-2} day^{-1}) (Table 1). The NPP values from VGPM and CbPM indicated significant overestimations. The coefficient of correlation (*r*) and standard error (SE) for *Eppley*-VGPM NPP values (r = 0.82 and SE = 116.16 mg C m^{-2} day^{-1}) were better than that obtained from the VGPM (r = 0.82 and SE = 203.69 mg C m^{-2} day^{-1}) and CbPM (r = 0.66 and SE = 142.84 mg C m^{-2} day^{-1}). Results suggested the *Eppley*-VGPM based NPP values match reasonably

well with the in-situ NPP. Therefore, we used the *Eppley*-VGPM model for the present study taking Aqua-MODIS as the input.

Table 1. Validation of ocean-colour based models (VGPM, *Eppley*-VGPM, and CbPM) with in-situ net primary production (mg C m^{-2} day^{-1}) estimated using ^{13}C tracer during the scientific expeditions to the Southern Ocean in 2009. CbPM- carbon based productivity model, VGPM- vertically generalized production model.

	r (coefficient of correlation)	Standard error	Bias	*p*-value
VGPM	0.82	203.69	104.40	0.001
Eppley-VGPM	0.82	116.16	-26.21	0.001
CbPM	0.66	142.84	94.14	0.026

We used monthly sea-ice concentration (SIC) data (September to November 2017) from the Special Sensor Microwave Imager Sounder (SSMIS) with spatial resolution of 25 km acquired from the National Snow and Ice Data Center (NSIDC) (Data id-G02135, Version 3). The data were generated using the NASA Team algorithm, which converts satellite derived brightness temperatures to gridded SIC (Cavalieri, D. J., C. L. Parkinson, P. Gloersen, 1997). A detail description about the sensor characteristics, sea-ice processing methods, synoptic coverage, resolution, projection, and validation of sea-ice retrieval from passive microwave sensors are given in earlier work (Fetterer et al., 2016). The polynya was interpreted when the pixel values found to be less than or equal to 15% of SIC (Fig. 3a-c) (Jena et al., 2019). In order to examine the role of oceanic processes for the formation of the phytoplankton bloom in the polynya, we used relevant physical oceanographic data. Metop-Advanced Scatterometer (ASCAT) wind stress curl and Ekman upwelling data (Pond, S., 1983) were acquired from the National Oceanic and Atmospheric Administration (NOAA) Coast watch (https://coastwatch.pfeg.noaa.gov) at a spatial resolution of 0.25° x 0.25° (Fig. 3g-l). Oceanic eddies were identified from the sea surface height anomaly (SSHA) and geostrophic currents (0.25° x 0.25°) derived from multi-mission merged satellite altimeter data (https://las.aviso.altimetry.fr/) (Fig. 3d-f) (Jena et al., 2019). Although the dipole structure of cyclonic and anticyclonic eddies was observed in the MR polynya, cyclonic eddies dominated the flow pattern in the region during the event. Therefore, we focused on the cyclonic eddies because they can upwell the deep warm and nutrient rich water to the upper ocean for the chl-*a* enhancement. The optimal interpolated sea surface temperature (OI SST) data (9 × 9 km) obtained from Remote Sensing Systems (www.remss.com), which was produced after merging of the microwave (cloud penetration capabilities) and infrared SST (high spatial resolution) using an OI scheme (Reynolds and Smith, 1994) (Fig. 3m-o). In order to understand the vertical structures of biophysical parameters, we used an Argo float (ID-5904468) data that had remained in the MR polynya from 2015 to 2017 (http://www.argo.ucsd.edu/) (Fig. 1a). The Argo based partial pressure of CO_2 (pCO_2) in the water column were calculated from a Deep-sea DuraFET pH sensor after using an existing algorithm for total alkalinity (Johnson et al., 2016). The uncertainty in the derived value is about 11 µatm at pCO_2 of 400 µatm (~2.7%),

considering the combined contribution from the pH sensor, the alkalinity estimate, and carbonate system equilibrium constants (Williams et al., 2017). The monthly incident shortwave radiation was acquired from the European Center for Medium-Range Weather Forecast (ECMWF) (grid resolution of 0.25°) during January 1979-December 2017. Monthly anomalies of shortwave radiation for September-November 2017 was computed relative to a 38-year climatology (1979-2016).

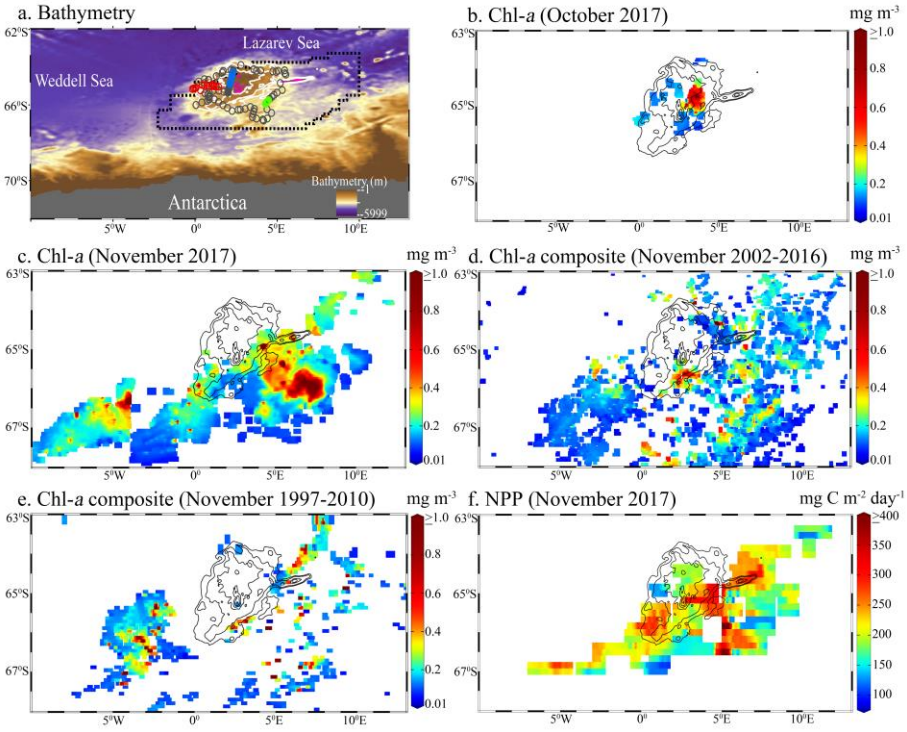
a. Bathymetry
Lazarev Sea
Weddell Sea
Antarctica
Bathymetry (m)
-1
-5999
b. Chl-a (October 2017)
mg m-3
c. Chl-a (November 2017)
d. Chl-a composite (November 2002-2016)
e. Chl-a composite (November 1997-2010)
f. NPP (November 2017)
mg C m-2 day-1
62°S
63°S
65°S
66°S
67°S
70°S
5°W
0°
5°E
10°E
≥1.0
0.8
0.6
0.4
0.2
0.01
≥400
350
300
250
200
150
100

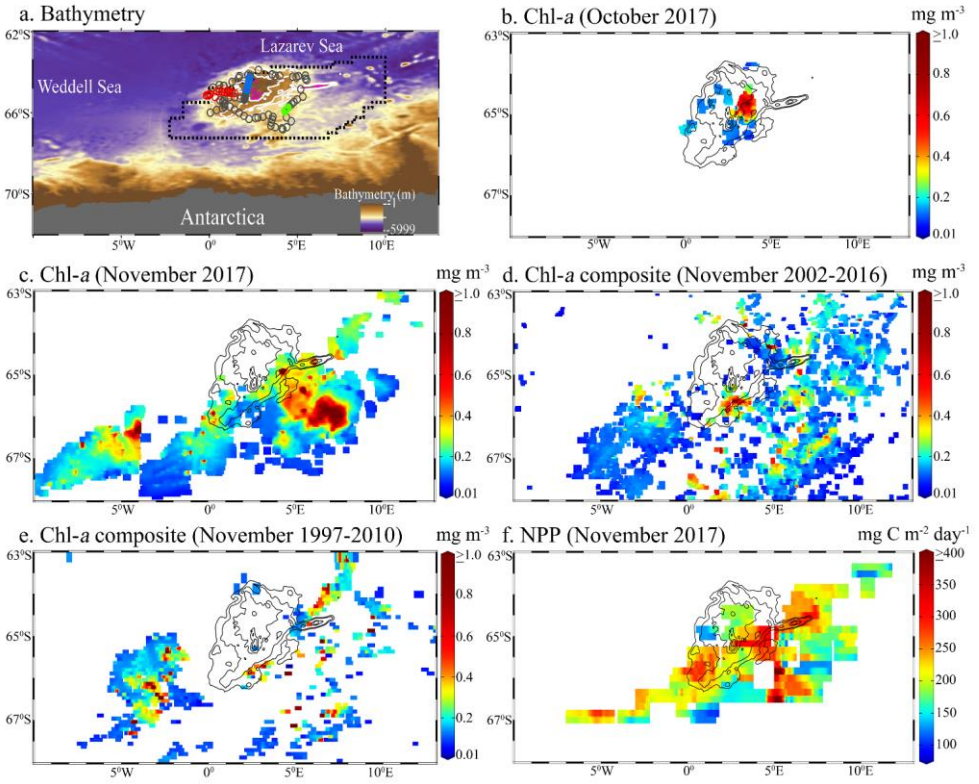
a. Bathymetry
Lazarev Sea
Weddell Sea
Antarctica
Bathymetry (m)
-1
-5999
b. Chl-a (October 2017)
mg m-3
c. Chl-a (November 2017)
d. Chl-a composite (November 2002-2016)
e. Chl-a composite (November 1997-2010)
f. NPP (November 2017)
mg C m-2 day-1
62°S
63°S
65°S
66°S
67°S
70°S
5°W
0°
5°E
10°E
≥1.0
0.8
0.6
0.4
0.2
0.01
≥400
350
300
250
200
150
100

Figure 1. (a) Bathymetry map of the Maud Rise from Earth Topography One Arc-Minute Global Relief Model, 2009. Pink lines show the depth contours shallower than 2000 m and other white contours are spaced by 500 m with deeper values. Dashed polygon shows the extent of the polynya during 21 November 2017. Circles represents the location of an ARGO float (ID-5904468) from 19 January 2015 to 18 March 2018. Red, green and blue circles show the float location from August to December, respectively for 2017, 2016 and 2015. (b) Monthly mean chlorophyll-*a* (chl-*a*) from Aqua-Moderate Resolution Imaging Spectroradiometer (Aqua-MODIS) during October 2017. (c) Monthly mean chl-*a* from Aqua-MODIS during November 2017. (d) Long-term composite of Aqua-MODIS chl-*a* (2002-2016) for November. (e) Long-term composite of SeaWiFS chl-*a* (1997-2010) for November. (f) Monthly mean daily net primary productivity (NPP) computed from the *Eppley*-vertically generalized production model for November 2017. The polyline features in figures b to f shows the extent of the Maud Rise seamount with a contour interval of 500 m.

3 Results and discussion

3.1 Phytoplankton bloom within the polynya

Although a large polynya was formed within the MR sea-ice cover during September 2017, no phytoplankton bloom observed in the satellite record. The polynya extent was nearly static from September to October and accompanied with a small patch of bloom (chl-*a* up to 3.48 mg m^{-3}) ~~centered~~centred at 3.77°E and 64.72°S (Fig. 1b; 3b), which remains otherwise covered by the sea-ice. Prior to the October 2017 event, no chl-*a* was observed ~~the satellite derived chl-*a* was missing~~ for the month of October from 1978 to 2016 even after considering entire data records of CZCS, SeaWiFS, Aqua-MODIS, and VIIRS. During November 2017, the polynya was enlarged and shifted southeastward with the high chl-*a* concentration reached up to 4.66 mg m^{-3} (Fig. 1c; 3c). The bloom was formed approximately between 4°E to 8°E, and 64.5°S to 66.5°S. Prior to the November 2017 event, the satellite derived chl-*a* observation was scarce (SeaWiFS and MODIS) and missing (CZCS and VIIRS) for the month of November from 1978 to 2016. Figures 1d and 1e shows the climatological composite of chl-*a* observations in November, respectively for Aqua-MODIS (2002-2016) and SeaWiFS (1997-2010). The scarce and missing observations were mainly due to the presence of seasonal sea-ice cover and cloud cover on the MR. The result suggests that the observed bloom from October to November 2017 had appeared for the first time within the MR polynya in the record of satellite observations since 1978 (Fig. 1b-c). Even though the monthly composite images shown the evidence of blooms, we processed Level-2 high spatial resolution scenes of Aqua-MODIS that provided more information on this unprecedented phytoplankton bloom. Several selected scenes that has relatively better coverage showed a patch of bloom on 25 October, followed by a wide band of bloom during 06 November and 21 November 2017 (Fig. 2). The chl-*a* values reached as high as 4.67 mg m^{-3} on 6 November 2017 (Fig. 2b). High diffuse attenuation coefficient (Kd 490) observed up to 0.39 m^{-1} and 0.37 m^{-1} during October and November, respectively, which is an indicator of sediment resuspension and bloom condition in the MR polynya (Table 2). The previously reported highest chl-*a* concentration in the Antarctic Polynya

have been identified in the Amundsen Sea (coastal polynya) with the values reached about 6.98 mg m^{-3} (Arrigo and Dijken, 2003). The bloom in the MR polynya was also tracked by a ~~fleet of~~ robotic Argo float (ID-5904468) that had remained at the north-western edge of the polynya (Fig. 1a; 4a). Result shows enhanced chl-*a* values from September to November 2017. The bloom condition was initiated on 25 October 2017 with the chl-*a* maxima up to 1.27 mg m^{-3} (36 m depth) at 0.86°E and 64.98°S (Fig. 4a). The chl-*a* value reached up to 1.31 mg m^{-3} (41 m depth) and 1.73 mg m^{-3} (36 m depth), respectively on 4 November and 14 November 2017. Further on 24 November 2017, the values reached as high as 5.47 mg m^{-3} (11 m depth) at 1.43°E and 65.04°S. In order to check whether this observed bloom is a seasonal or an episodic feature of the MR, we analyzed the Argo float data during two preceding years of 2015 and 2016 when the sea-ice was covered. Analysis shows that the bloom was absent and the chl-*a* value found to be rather low during October and November for 2015 and 2016 (Fig. 4b,c). Thus, the result confirms that the observed bloom in 2017 was an unprecedented feature considering both the Argo float and multi-sensor satellite data.

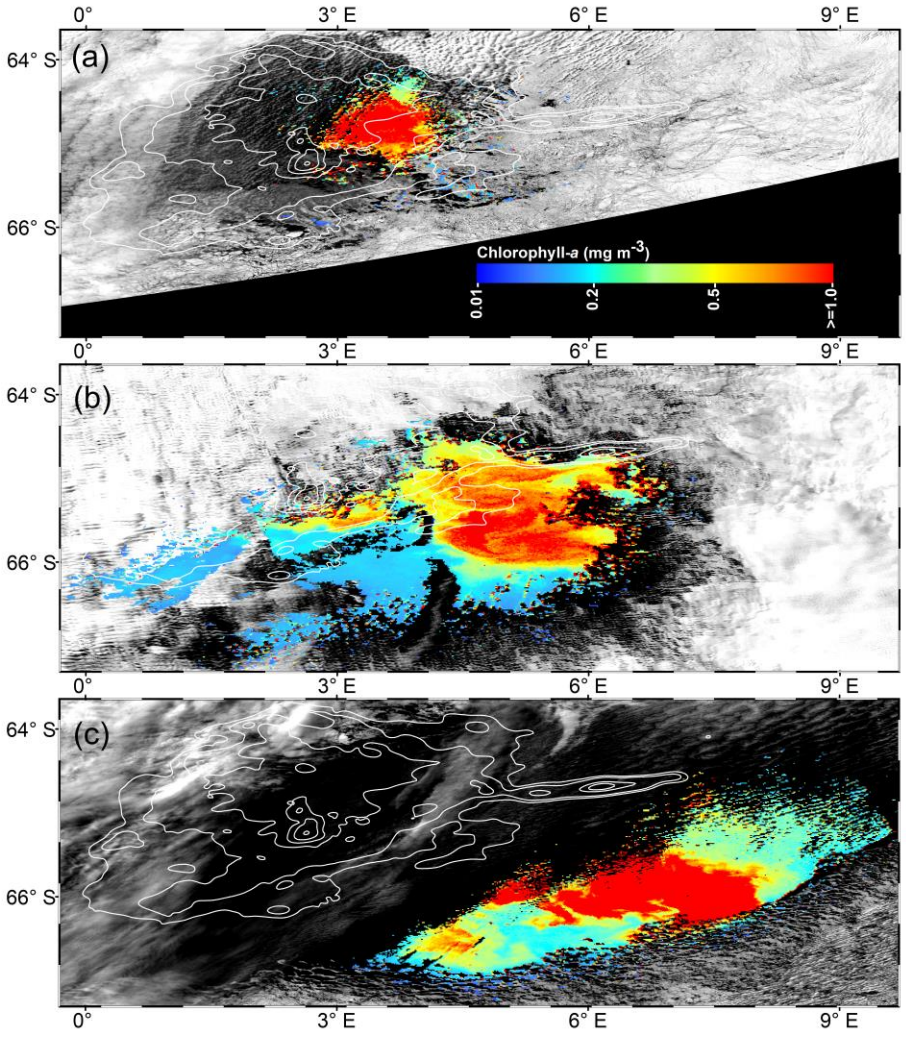
0°
3° E
6° E
9° E
64° S
66° S
(a)
Chlorophyll-a (mg m-3)
0.01
0.2
0.5
>=1.0
(b)
(c)

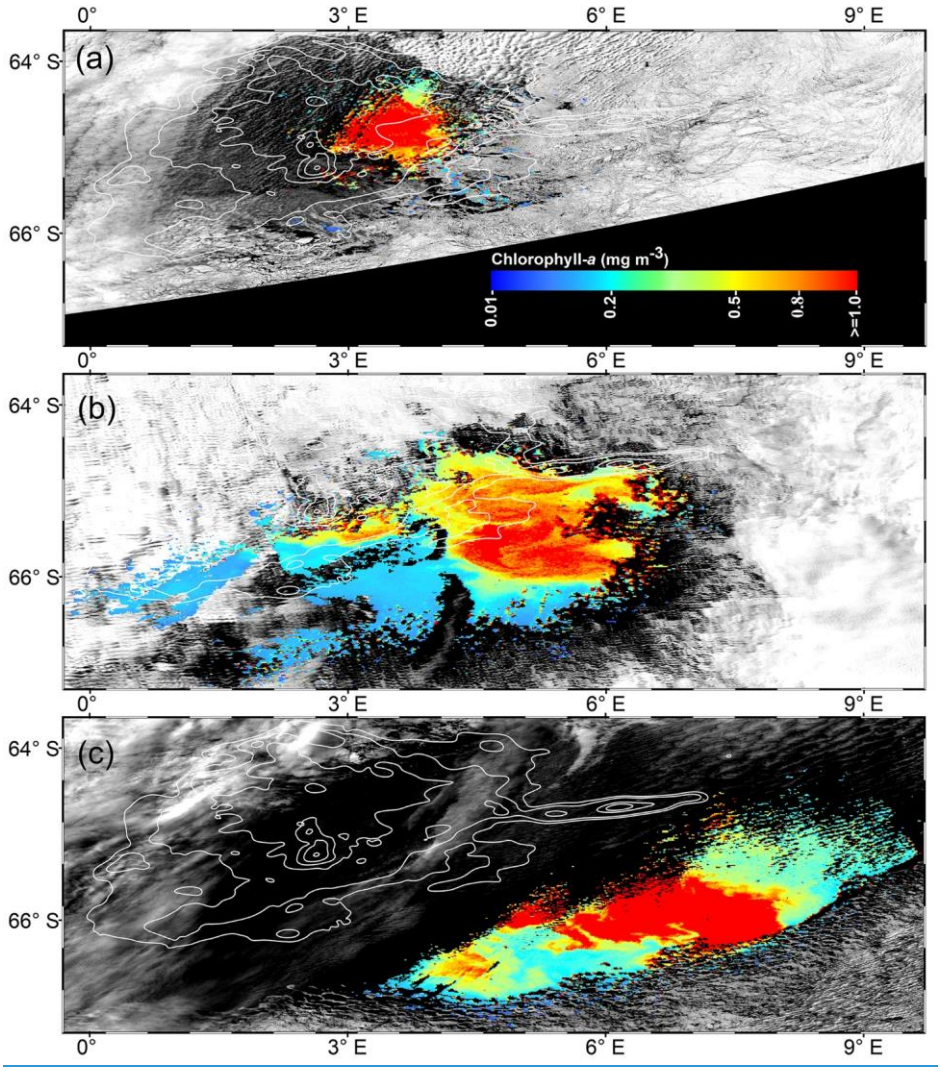
0°
3° E
6° E
9° E
64° S
66° S
(a)
Chlorophyll-a (mg m-3)
0.01
0.2
0.5
0.8
>=1.0
(b)
(c)

Figure 2. High spatial resolution (~1 km) Aqua-MODIS ascending passes during (a) 25 October (14:45 hours), (b) 06 November (15:05 hours), and (c) 21 November 2017 (14:25 hours), showing the unprecedented phytoplankton blooms in the Maud Rise polynya. The white contours show the extent of the Maud Rise seamount.

3.2 Causes of the observed bloom formation

Generally, the phytoplankton biomass remains low in the SO which is mainly ascribed to the lack of micronutrient iron apart from strong zooplankton grazing pressure, light and silicate limitation (de Baar and Boyd, 1999; Boyd et al., 2001; Gall et al., 2001; Selph et al., 2001). The input of iron-enriched atmospheric dust from the continents to the SO is the lowest in the world's oceans (Duce and Tindale, 1991); and the oceanic sources of iron from the deep water and vertical diffusion of iron through the water column have been reported as the likely pathways of iron supply to the upper ocean (Jena, 2016; Tagliabue et al., 2014). The occurrence of phytoplankton bloom is possible over the shallow regions of MR seamount where the doming of isotherm/isopycnal can bring deeper high-nutrient water above the seamount where it may be utilised with a conducive environment of light availability and water column stability (White and Mohn, 2002). Analysis of bathymetric data indicated the peak of the MR seamount is located at 2.63°E, 65.23°S, that rises from the abyssal plain of ~5200 m to the shallowest depth of ~968 m (Fig. 1a), influencing the local upliftment of thermocline and nutrient enriched deep-water (Jena et al., 2019; Mashayek et al., 2017; Muench et al., 2001; Roden, 2013). However, the oceanic processes that can bring subsurface nutrients to the sea surface have an important role for the formation of phytoplankton bloom. In order to examine the role of oceanic processes, we used satellite derived physical oceanographic data as shown in Fig. 3.

Analysis of monthly SSHA and corresponding geostrophic currents showed the presence of a large cyclonic eddy with a diameter of ~220 km in the vicinity of MR seamount during September 2017 (Fig. 3d). The center of the cyclonic eddy was located approximately at 3.84°E and 64.47°S, closely matching with the center of the polynya having warm SST (-1.35°C) compared to its peripheral cold SST of -1.79°C (Fig. 3d; 3m). The polynya extent was nearly static from September to October. During November, the polynya expanded southeastward in conjunction with the movement of cyclonic eddy accompanied by a pool of warm SST and the phytoplankton bloom (Fig. 1c; 3f; 3o). The eddy was located approximately at 3.96°E and 66.5°S in November. Even though a dipole structure of cyclonic and anticyclonic eddies was observed in the polynya, a large cyclonic eddy dominated the flow pattern. The location of cyclonic eddy matching well with the annular halo of warm SST and patch of phytoplankton bloom in the polynya (Fig. 1b-c; 3d-f; 3m-o). In addition, we find that the polynya surface was associated with persistent negative wind stress curl (Fig. 3g-i) that induced upwelling of sub-surface water to the sea surface during September-November 2017 (Fig. 2j-l). Generally, the water column on the MR seamount is characterized by the presence of a cold fresh layer in the upper ocean separated from a lower warm saline layer by a weak pycnocline (Jena et al., 2019; de Steur et al., 2007). The combined influence of the cyclonic eddy and negative wind stress curl brings up the warm thermocline water into the sea surface through Ekman upwelling that results in a pool of warm SST at the polynya center (Fig. 3m-o). Depth-Latitude cross section of the Copernicus Marine Environment Monitoring Service

(CMEMS) global analysis and forecast data on potential temperature data at a polynya location (along 4.7°E) provided evidence that the subsurface warm water was ventilated and brought closer to the upper ocean from the thermocline (upward doming of isotherms) during September through November 2017 (Jena et al., 2019) (Fig. S3). The Argo float located at the edge of the polynya also provided evidence on the upliftment of thermocline during September 2017 (Fig. ~~S4~~5). Ocean upwelling is known to supply dissolved iron to the upper ocean (Klunder et al., 2014; Rosso et al., 2014), preferably at the shallow bathymetry of less than 1 km at the MR seamount (Graham et al., 2015). Synchronously, along with the availability of light in October and November, the observed mechanism triggered a bloom condition in the MR polynya (Fig. 1b-c; 2a-c). ARGO float indicated mixed layer warming on the Maud Rise during spring 2016 and 2017 (Fig. S4~~5~~). The upwelling of high saline and warm water into the mixed layer facilitated the sea-ice melting. The melting of sea-ice leads to the development of shallow mixed layer due to the accumulation of freshwater in the upper ocean. Therefore, we observed lower values of salinity in the mixed layer with increased stability of the water column (Fig. S4~~5~~). The development of shallow mixed layer improved the light availability in the upper ocean and the condition was ~~favorable~~favourable for the growth of phytoplankton. Even though the Ekman upwelling was evident in September, the bloom did not appear in the polynya region under low light condition up to 12.6 Einstein m^{-2} day^{-1}. However, the bloom was appeared in October-November 2017 under the influence of Ekman upwelling and improved light condition up to 36.1 and 61.9 Einstein m^{-2} day^{-1}, respectively for October and November (Fig. S5~~6~~; Table 2). Analysis of incident shortwave radiation data shows record highest gain of values in the polynya region during September-November 2017, considering the 38-year time series starting from 1979 through 2016 (Fig. S6). The observed anomalous gain in net shortwave radiation is possibly due to the early loss of sea ice cover.

Formatted: English (United Kingdom)

Computation of NPP using the *Eppley*-VGPM model indicated the carbon fixation rates in the MR polynya varied between 60.08 and 374.07 mg C m^{-2} day^{-1}, with an average value of 169.51 mg C m^{-2} day^{-1} for October 2017 (Table 2). The NPP increased in November that ranged from 101.43 to 415.08 mg C m^{-2} day^{-1}, averaging 208.44 mg C m^{-2} day^{-1} with the highest rate being observed at 5.16°E and 66.58°S. The observed values in the polynya remained within the previously reported range for the Polar Frontal Zone of the SO (100-6000 mg C m^{-2} day^{-1}) (Hoppe et al., 2017; Korb and Whitehouse, 2004; Mitchell and Holm-Hansen, 1991; Moore and Abbott, 2000; Park et al., 2010). The results from Aqua-MODIS observations in the Antarctic coastal polynyas indicated that the NPP values ranged from 34.3 to 911.9 mg C m^{-2} day^{-1} during November 2017 with the highest rate being observed at Sulzberger Bay polynya (Ross Sea) at 155.33°W and 76.08°S (Table 3). The NPP values in the MR polynya remained within the range of similar values observed for the coastal polynyas. The NPP values varied from 90 to 760 mg C m^{-2} day^{-1} for 37 coastal polynyas around the Antarctica (Arrigo and Dijken, 2003). Even though the phytoplankton bloom was appeared in the MR polynya with the NPP values similar to those of coastal polynyas, the spatial variation of NPP did not follow always the same pattern of chl-*a* (Figs. 1c; 1f). The observed pattern has been attributed to the effect of phytoplankton pigment composition and packaging (Bricaud et al., 2004; Ciotti et al., 2002; Jena, 2017; Lohrenz et al., 2003; Marra et al., 2007; Morel and Bricaud, 1981). The primary production in the upper ocean is a

function of chl-*a*, availability of light, nutrients, phytoplankton-specific absorption coefficient (capacity of light absorption), and the efficiency of phytoplankton to convert the absorbed light for the carbon fixation (Behrenfeld and Falkowski, 1997a). However, the capacity of light absorption and the quantum yield of photosynthetic carbon fixation would vary from one phytoplankton community to another (Claustre et al., 2005). Although, the primary production in the Antarctic coastal polynyas are known to be dominated by prymnesiophytes (Phaeocystis antarctica) or diatoms (Arrigo et al., 2008b), the data on the phytoplankton community structure and their spectral characteristics are not available for the analysis in order to quantify the rate of carbon fixation for individual community.

Table 2. Net primary production and bio-optical parameters during the occurrence of Maud Rise polynya in October and November 2017. Values for November 2017 are given within brackets. NPP: Net primary production, Chl-*a*: Chlorophyll-*a*, Eu: Euphotic depth, PAR: Photosynthetically available radiation, Kd: Diffuse attenuation coefficient for downwelling irradiance, SST: Sea surface temperature.

	Minimum	Maximum	Mean	Standard deviation
NPP (mg C m^{-2} day^{-1})	60.08 (101.43)	374.07 (415.08)	169.51 (208.44)	84.04 (50.90)
Chl-*a* (mg m^{-3})	0.07 (0.06)	3.48 (4.67)	0.29 (0.28)	0.26 (0.20)
Eu (m)	27.12 (8.35)	84.24 (109.56)	53.72 (56.90)	13.59 (12.49)
PAR (Einstein m^{-2} day^{-1})	6.27 (13.80)	36.10 (61.90)	17.79 (31.43)	6.86 (8.21)
Kd 490 (m^{-1})	0.03 (0.02)	0.39 (0.37)	0.06 (0.06)	0.03 (0.02)
SST (°C)	-1.80 (-1.80)	-1.25 (-1.31)	-1.67 (-1.65)	0.12 (0.14)

Table 3. Net primary production (mg C m^{-2} day^{-1}) for some coastal polynyas around the Antarctica in November 2017. The values in the parentheses indicates locational information.

	Minimum	Maximum	Mean	Standard deviation
Amundsen Bay, Enderby Land	34.3 (50.25°E,66.75°S)	55.9 (50.58°E,67.08°S)	44.7	6.5
Barrier, Prydz Bay	161.8 (79.25°E,67.08°S)	505.5 (80.25°E,67.08°S)	308.5	93.2
Vincennes Bay	53.17 (108.83°E,66.83°S)	68.9 (108.66°E,66.91°S)	61.5	5.3
Wrigley Gulf, Amundsen Sea	52.5 (125.66°W,73.33°S)	74.0 (125.58°W,73.41°S)	67.2	6.8
Sulzberger Bay, Ross Sea	251.9 (154.33°W,75.91°S)	911.9 (155.33°W,76.08°S)	606.6	143.8

Formatted: Font color: Auto
Formatted: Font color: Auto
Formatted: Font color: Auto
Formatted: Font color: Auto
Formatted: Font color: Auto
Formatted: Font color: Auto

Further, Argo data were utilized to find the linkage between the observed bloom and the ocean pCO_2 condition. Analysis of Argo data indicated low pCO_2 values that reached as low as 372.8 µatm (Fig. 4d) corresponding to the occurrence of bloom during October-November 2017 (Fig. 4a). The pCO_2 values declined during the occurrence of bloom in comparison with the period of non-bloom condition in August-September 2017, 2015 and 2016 (Fig. 4). The coefficient of correlation (r) between the pCO_2 and chl-*a* was -0.56 ($p < 0.01$) during August-September 2017 (Fig. S7~~7~~5a). The relationship improved ($r = -0.82$, $p < 0.01$) and the spatial pattern closely matched together during the bloom condition in October-November 2017 (Fig. S7~~7~~5b; 4a-d). The best relationship observed between the pCO_2 and chl-*a* when the data was log transformed ($r = -0.94$, $p < 0.01$). The observed low pCO_2 values in the polynya was likely due to the presence of chl-*a* bloom with high NPP, which has potential to drive CO_2 fluxes from the atmosphere to the ocean after forming a pressure gradient. This biological pumping process in the polynya could play an important role for lowering the atmospheric CO_2 through transferring of atmospheric CO_2 to the ocean and subsequently into the ocean sediments. However, it is important to mention that the air-sea exchange of CO_2 is driven by the pCO_2 gradient, solubility of CO_2 in the seawater (function of ocean temperature and salinity), and gas transfer velocity (function of wind speed and SST) (Williams et al., 2017). Follow-up research works are required in the future to quantify the contribution from physical and biological processes for explaining the air-sea exchange of CO_2 in the MR polynya and its likely role in regulating the global climate (Gordon and Comiso, 1988; Li et al., 2016).

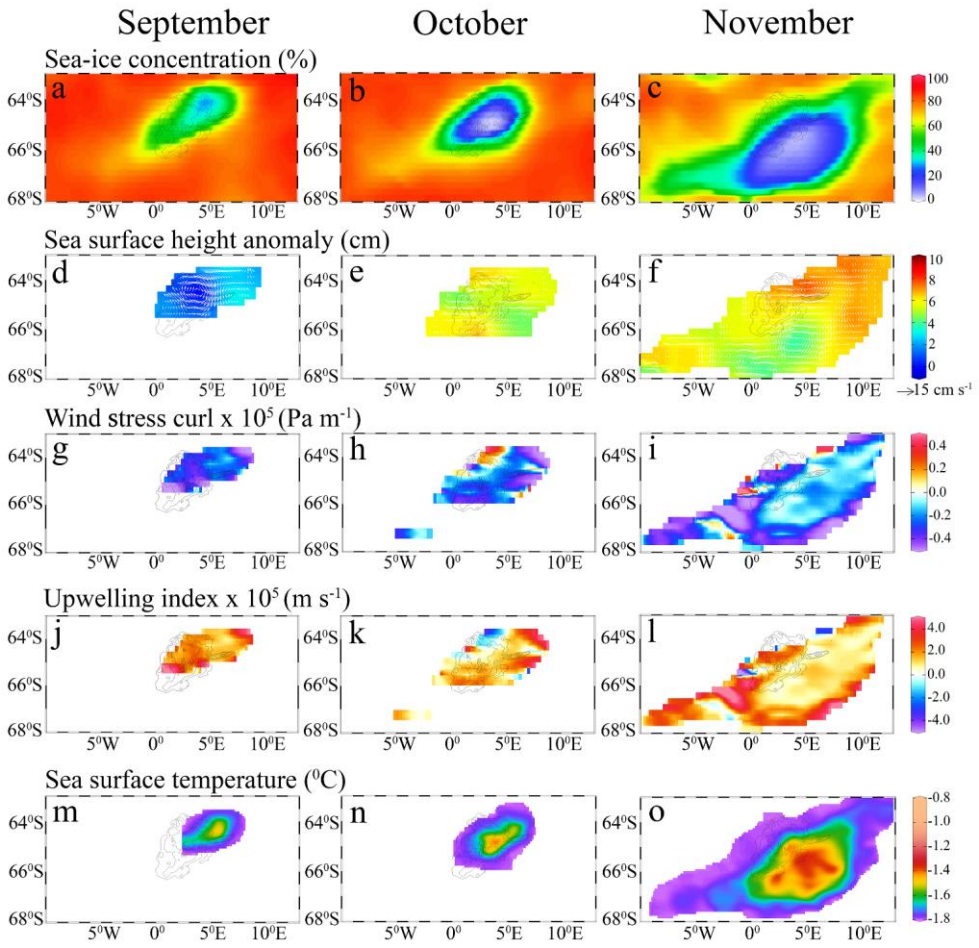

Figure 3. Monthly maps show (a-c) sea-ice concentration, (d-f) sea surface height anomaly and geostrophic current velocity (white arrows), (g-i) wind stress curl, (j-l) upwelling index, and (m-o) sea surface temperature variability during the appearance of polynya from September to November 2017.

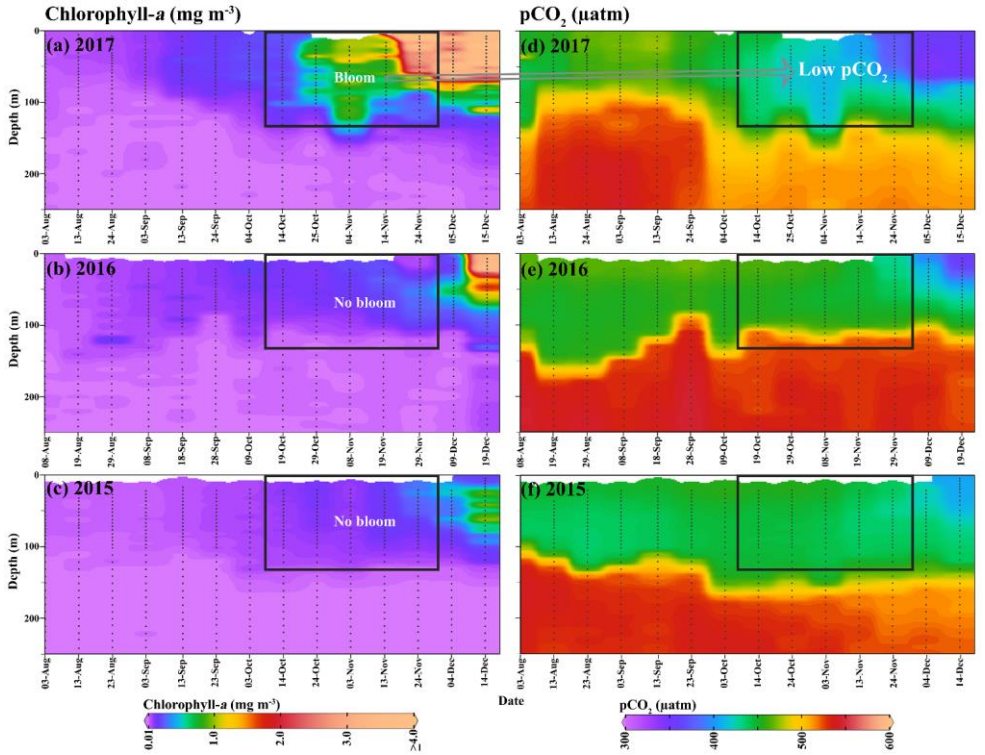

Figure 4. An Argo float (ID-5904468) located on the Maud Rise seamount shows profiles of (a-c) chlorophyll-*a*, and (d-f) pCO_2 from August to December (2015-2017). Marked rectangle in figure-4a shows the bloom condition from October to November 2017, and the bloom was absent during respective period of two preceding years (2015 and 2016). Low pCO_2 values observed corresponding to the bloom occurrence.

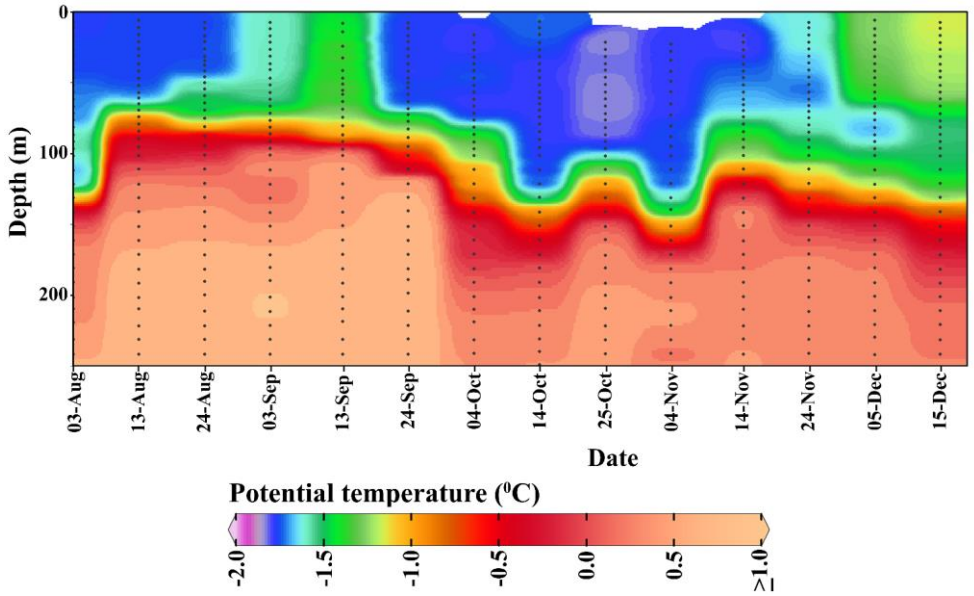

Figure 5. Potential temperature profile from an Argo float (ID-5904468) located at the edge of the Maud Rise polynya during August-December 2017.

4 Summary and conclusion

In this article, we have shown that the phytoplankton bloom occurred on the MR seamount during the appearance of polynya in spring 2017. Analysis of multi-sensor satellite data from CZCS, SeaWiFS, MODIS, and VIIRS indicated that the bloom appeared for the first time in the satellite records since 1978. Since there is no previous report of its occurrence in the MR polynya, we have examined additional data from Argo float for a firm evidence. The ARGO float located at the north-western edge of the polynya provided evidence of bloom condition from October to November 2017 compared to the preceding years of 2015 and 2016 when the sea-ice was covered at the surface with low chl-*a*. We find that the combined influence of seamount and physical processes are accountable for the formation of the observed bloom. The presence of a seamount on the MR leads to upliftment of thermocline and nutrient enriched deep water that could fertilize the upper ocean through support of upwelling process. During the austral winter and spring 2017, the supply of nutrient to the upper ocean arises through Ekman upwelling driven by a large cyclonic ocean eddy and the persistent negative wind stress curl. Even though the Ekman upwelling was evident in September 2017, the bloom did not appear in the polynya due to prevailing low

irradiance as expected in an austral winter. However, the bloom was appeared in austral spring (October-November 2017) under the influence of Ekman upwelling and improved light condition that favored for the phytoplankton photosynthesis and growth. Low pCO_2 condition prevailed in the polynya due to the presence of chl-*a* bloom with high NPP that can lead to sinking of atmospheric CO_2 fluxes into the ocean. The observed phytoplankton bloom reported in this article has large importance considering the HNLC status of the SO.

Studies have shown intensification of polar cyclone activities due to the poleward shifting of the extratropical cyclone track in the background of a warming climate condition (Francis et al., 2019; Fyfe, 2003). As the polar cyclones are known to trigger the occurrence of polynyas (Francis et al., 2019; Jena et al., 2019; Turner et al., 2017) (through advection of moist-warm air from extratropic, and sea-ice divergence), the frequency of polynya event is likely to be increased in the future (including over the MR) under a warming climate condition. The likelihood for the occurrence of the polynya is quite high with a background of anomalous upper ocean warming and sea-ice loss, similar to the events that occurred in the Antarctic sea-ice from 2016 to 2019 (Fig. S1). Indeed, the Weddell Sea and MR polynya has reappeared in 23 November 2018 that lasted till 12 December 2018 as observed from SSMIS (Fig. S8~~6~~). With the frequent reoccurrence of polynya on the MR, the associated physical processes could possibly modify the region into a productive environment and likely to have impact on the regional ecosystem and carbon cycle. The occurrence of polynya and phytoplankton blooms in the MR may lead it to a site of potential sink of atmospheric CO_2 through biological pumping and can be a major source of carbon and energy for the regional food web. The spatial dimension of the bloom in a polynya might be small; however, it is necessary to monitor and understand as many important features of the Antarctic marine ecosystem in order to understand its complete role in the global biogeochemical cycle. The study demonstrates how the phytoplankton in the Southern Ocean (specifically over the shallow bathymetric region) would likely respond in the future under a warming climate condition and continued melting of Antarctic sea-ice since austral spring 2016.

Code/Data availability

We have analyzed monthly sea-ice concentration (SIC) data (September to November 2017) from the passive microwave sensors with spatial resolution of 25 km acquired from the National Snow and Ice Data Center (NSIDC) (Data id-G02135, Version 3, https://nsidc.org/data). The data were generated using the NASA Team algorithm, which converts satellite derived brightness temperatures to gridded SIC (Cavalieri, D. J., C. L. Parkinson, P. Gloersen, 1997). We used ocean potential temperature data from global marine Argo atlas (http://www.argo.ucsd.edu/Marine_Atlas.html#) that indicated anomalous upper ocean warming of the Southern Ocean from 2016 to 2018. In order to analyze the Aqua-MODIS derived net primary production (NPP), we have validated three ocean-color based models such as the vertically generalized production model (VGPM), *Eppley*-VGPM, and carbon-based productivity model (CbPM) for selecting the best model for the study region. The model based NPP values were available in weekly time scale with a spatial resolution of ~4 km (https://www.science.oregonstate.edu/ocean.productivity). We analysed eddy-resolving model data available from

Copernicus Marine Environment Monitoring Service (CMEMS) global analysis and forecast (http://marine.copernicus.eu/services-portfolio/access-to-products/, GLOBAL_ANALYSIS_FORECAST_PHY_001_024). The detailed methodology of product generation, and quality control approaches for this data is given online at http://cmems-resources.cls.fr/documents/QUID/CMEMS-GLO-QUID-001-024.pdf. Hydrographic profiles from an Argo float (ID-5904468) located at the edge of the Maud Rise polynya were analyzed for August-December 2017. The Argo data are being generated from the Southern Ocean Carbon and Climate Observations and Modeling (SOCCOM) Project funded by the National Science Foundation, Division of Polar Programs (NSF PLR -1425989), supplemented by NASA, and by the International Argo Program and the NOAA programs. The data are available at https://www.mbari.org/science/, http://www.argo.ucsd.edu/, http://argo.jcommops.org/. The primary production data used for the validation are available at https://data.mendeley.com/ data repository under doi: 10.17632/k438knz9zs.5.

Author contributions

BJ. All works are carried out by BJ except the validation experiment of ocean color data using in-situ observations from the Southern Ocean expeditions.

NAK. Validation of ocean color data using in-situ observations from the Southern Ocean expeditions, revision of the manuscript.

Competing interests

The authors declare no conflict of interest.

Acknowledgments

The authors are thankful to the Director, NCPOR, for his continuous support. The author greatly acknowledges various organizations such as the National Snow and Ice Data Center (NSIDC), National Oceanic and Atmospheric Administration (NOAA), National Aeronautics and Space Administration (NASA) Goddard Space Flight Center (Ocean Biology Processing Group), Copernicus Marine Environment Monitoring Service (CMEMS), and their data processing teams for making various datasets available in their portals. Argo data were available from the Southern Ocean Carbon and Climate Observations and Modeling (SOCCOM) Project funded by the National Science Foundation, Division of Polar Programs (NSF PLR -1425989), supplemented by NASA, and by the International Argo Program and the NOAA programs (http://www.argo.ucsd.edu, http://argo.jcommops.org). We also acknowledge N. Gandhi, IITM, for providing the in-situ primary production data.

References

Alderkamp, A.-C., Mills, M. M., van Dijken, G. L., Laan, P., Thuróczy, C.-E., Gerringa, L. J. A., de Baar, H. J. W., Payne, C. D., Visser, R. J. W., Buma, A. G. J. and Arrigo, K. R.: Iron from melting glaciers fuels phytoplankton blooms in the Amundsen Sea (Southern Ocean): Phytoplankton characteristics and productivity, Deep Sea Research Part II: Topical

Studies in Oceanography, 71–76, 32–48, doi:https://doi.org/10.1016/j.dsr2.2012.03.005, 2012.

Ardelan, M. V., Holm-Hansen, O., Hewes, C. D., Reiss, C. S., Silva, N. S., Dulaiova, H., Steinnes, E. and Sakshaug, E.: Natural iron enrichment around the Antarctic Peninsula in the Southern Ocean, Biogeosciences, 7(1), 11–25, doi:10.5194/bg-7-11-2010, 2010.

Arrigo, K. R. and Alderkamp, A.-C.: Shedding dynamic light on Fe limitation (DynaLiFe), Deep Sea Research Part II: Topical Studies in Oceanography, 71–76, 1–4, doi:10.1016/j.dsr2.2012.03.004, 2012.

Arrigo, K. R. and Dijken, G. L. van: Phytoplankton dynamics within 37 Antarctic coastal polynya systems, Journal of Geophysical Research, 108(C8), 3271, doi:10.1029/2002jc001739, 2003.

Arrigo, K. R., van Dijken, G. and Long, M.: Coastal Southern Ocean: A strong anthropogenic CO2 sink, Geophysical Research Letters, 35(21), doi:10.1029/2008GL035624, 2008a.

Arrigo, K. R., van Dijken, G. L. and Bushinsky, S.: Primary production in the Southern Ocean, 1997–2006, Journal of Geophysical Research: Oceans, 113(C8), doi:10.1029/2007JC004551, 2008b.

de Baar, H. J. W. and Boyd, P. M.: The Role of Iron in Plankton Ecology and Carbon Dioxide Transfer of the Global Oceans, in The Dynamic Ocean Carbon Cycle: A Midterm Synthesis of the Joint Global Ocean Flux Study, edited by R. B. Hanson, H. W. Ducklow, and J. G. Field, pp. 61–140, Cambridge University Press., 1999.

Bates, N. R., Hansell, D. A., Carlson, C. A. and Gordon, L. I.: Distribution of CO2 species, estimates of net community production, and air-sea CO2 exchange in the Ross Sea polynya, Journal of Geophysical Research: Oceans, 103(C2), 2883–2896, doi:10.1029/97JC02473, 1998.

Behrenfeld, M. J. and Falkowski, P. G.: A consumer's guide to phytoplankton primary productivity models, Limnology and Oceanography, 42(7), 1479–1491, doi:10.4319/lo.1997.42.7.1479, 1997a.

Behrenfeld, M. J. and Falkowski, P. G.: Photosynthetic rates derived from satellite-based chlorophyll concentration, Limnology and Oceanography, 42(1), 1–20, doi:10.4319/lo.1997.42.1.0001, 1997b.

Boyd, P. W., Crossley, A. C., DiTullio, G. R., Griffiths, F. B., Hutchins, D. A., Queguiner, B., Sedwick, P. N. and Trull, T. W.: Control of phytoplankton growth by iron supply and irradiance in the subantarctic Southern Ocean: Experimental results from the SAZ Project, Journal of Geophysical Research: Oceans, 106(C12), 31573–31583, doi:10.1029/2000JC000348, 2001.

Bricaud, A., Babin, M., Morel, A. and Claustre, H.: Variability in the chlorophyll-specific absorption coefficients of natural phytoplankton: Analysis and parameterization, Journal of Geophysical Research, 100(C7), 13321, doi:10.1029/95jc00463, 2004.

Cassar, N., Bender, M. L., Barnett, B. A., Fan, S., Moxim, W. J., Levy, H. and Tilbrook, B.: The Southern Ocean Biological Response to Aeolian Iron Deposition, Science, 317(5841), 1067–1070, doi:10.1126/science.1144602, 2007.

Cavalieri, D. J., C. L. Parkinson, P. Gloersen, and H. J. Z.: Arctic and Antarctic Sea Ice Concentrations from Multichannel Passive-Microwave Satellite Data Sets: October 1978-September 1995 - User's Guide. NASA TM 104647., Greenbelt, MD 20771., 1997.

Ciotti, Á. M., Lewis, M. R. and Cullen, J. J.: Assessment of the relationships between dominant cell size in natural phytoplankton communities and the spectral shape of the absorption coefficient, Limnology and Oceanography, 47(2), 404–

417, doi:10.4319/lo.2002.47.2.0404, 2002.

Claustre, H., Babin, M., Merien, D., Ras, J., Prieur, L., Dallot, S., Prasil, O., Dousova, H. and Moutin, T.: Toward a taxon-specific parameterization of bio-optical models of primary production: A case study in the North Atlantic, Journal of Geophysical Research: Oceans, 110(C7), doi:10.1029/2004JC002634, 2005.

Duce, R. A. and Tindale, N. W.: Atmospheric transport of iron and its deposition in the ocean, Limnology and Oceanography, 36(8), 1715–1726, doi:10.4319/lo.1991.36.8.1715, 1991.

Eppley, Richard: Temperature and phytoplankton growth in the sea., Fishery Bulletin, 70(4), 1063–1085 [online] Available from: http://lgmacweb.env.uea.ac.uk/green_ocean/publications/Nano/Eppley72.pdf, 1972.

Fetterer, F., Knowles, K., Meier, W. and Savoie, M.: Sea Ice Index, Version 2 (updated daily), Boulder, Colorado USA., 2016.

Fitch, D. T. and Moore, J. K.: Wind speed influence on phytoplankton bloom dynamics in the Southern Ocean Marginal Ice Zone, Journal of Geophysical Research: Oceans, 112(C8), doi:10.1029/2006JC004061, 2007.

Francis, D., Eayrs, C., Cuesta, J. and Holland, D.: Polar Cyclones at the Origin of the Reoccurrence of the Maud Rise Polynya in Austral Winter 2017, Journal of Geophysical Research: Atmospheres, 124(10), 5251–5267, doi:10.1029/2019JD030618, 2019.

Fyfe, J. C.: Extratropical Southern Hemisphere cyclones: Harbingers of climate change?, Journal of Climate, 16(17), 2802–2805, doi:10.1175/1520-0442(2003)016<2802:ESHCHO>2.0.CO;2, 2003.

Gall, M. P., Boyd, P. W., Hall, J., Safi, K. A. and Chang, H.: Phytoplankton processes. Part 1: Community structure during the Southern Ocean Iron RElease Experiment (SOIREE), Deep Sea Research Part II: Topical Studies in Oceanography, 48(11), 2551–2570, doi:https://doi.org/10.1016/S0967-0645(01)00008-X, 2001.

Gandhi, N., Ramesh, R., Laskar, A. H., Sheshshayee, M. S., Shetye, S., Anilkumar, N., Patil, S. M. and Mohan, R.: Zonal variability in primary production and nitrogen uptake rates in the southwestern Indian Ocean and the Southern Ocean, Deep-Sea Research Part I: Oceanographic Research Papers, 67, 32–43, doi:10.1016/j.dsr.2012.05.003, 2012.

Gordon, A. L. and Comiso, J. C.: Polynyas in the Southern Ocean the global heat engine that couples the ocean and the atmosphere, Scientific American, 258(6), 90–97, 1988.

Graham, R. M., Boer, A. M. De, van Sebille, E., Kohfeld, K. E. and Schlosser, C.: Inferring source regions and supply mechanisms of iron in the Southern Ocean from satellite chlorophyll data, Deep Sea Research Part I: Oceanographic Research Papers, 104, 9–25, doi:https://doi.org/10.1016/j.dsr.2015.05.007, 2015.

Hoppe, C. J. M., Wolf-Gladrow, D. A., Trimborn, S., Strass, V., Soppa, M. A., Cheah, W., Rost, B., Bracher, A., Santos-Echeandia, J., Laglera, L. M., Hoppema, M., Klaas, C. and Ossebaar, S.: Controls of primary production in two phytoplankton blooms in the Antarctic Circumpolar Current, Deep Sea Research Part II: Topical Studies in Oceanography, 138, 63–73, doi:10.1016/j.dsr2.2015.10.005, 2017.

Jena, B.: Satellite remote sensing of the island mass effect on the Sub-Antarctic Kerguelen Plateau, Southern Ocean, Frontiers of Earth Science, 10(3), 479–486, doi:10.1007/s11707-016-0561-8, 2016.

Jena, B.: The effect of phytoplankton pigment composition and packaging on the retrieval of chlorophyll-a concentration from satellite observations in the Southern Ocean, International Journal of Remote Sensing, 38(13), 3763–3784,

doi:10.1080/01431161.2017.1308034, 2017.

Jena, B., Ravichandran, M. and Turner, J.: Recent Reoccurrence of Large Open-Ocean Polynya on the Maud Rise Seamount, Geophysical Research Letters, 46(8), 4320–4329, doi:10.1029/2018GL081482, 2019.

Johnson, K. S., Jannasch, H. W., Coletti, L. J., Elrod, V. A., Martz, T. R., Takeshita, Y., Carlson, R. J. and Connery, J. G.: Deep-Sea DuraFET: A Pressure Tolerant pH Sensor Designed for Global Sensor Networks, Analytical Chemistry, 88(6), 3249–3256, doi:10.1021/acs.analchem.5b04653, 2016.

Johnson, R., Strutton, P. G., Wright, S. W., McMinn, A. and Meiners, K. M.: Three improved satellite chlorophyll algorithms for the Southern Ocean, Journal of Geophysical Research: Oceans, 118(7), 3694–3703, doi:10.1002/jgrc.20270, 2013.

Kahru, M., Mitchell, B. G., Gille, S. T., Hewes, C. D. and Holm-Hansen, O.: Eddies enhance biological production in the Weddell-Scotia Confluence of the Southern Ocean, Geophysical Research Letters, 34(14), doi:10.1029/2007GL030430, 2007.

Kahru, M., Lee, Z., Mitchell, B. G. and Nevison, C. D.: Effects of sea ice cover on satellite-detected primary production in the Arctic Ocean, Biology Letters, 12(11), 20160223, doi:10.1098/rsbl.2016.0223, 2016.

Klunder, M. ~B., Laan, P., De Baar, H. ~J. ~W., Middag, R., Neven, I. and Van Ooijen, J.: Dissolved Fe across the Weddell Sea and Drake Passage: impact of DFe on nutrient uptake, Biogeosciences, 11, 651–669, doi:10.5194/bg-11-651-2014, 2014.

Korb, R. E. and Whitehouse, M.: Contrasting primary production regimes around South Georgia, Southern Ocean: Large blooms versus high nutrient, low chlorophyll waters, Deep-Sea Research Part I: Oceanographic Research Papers, 51(5), 721–738, doi:10.1016/j.dsr.2004.02.006, 2004.

Labrousse, S., Williams, G., Tamura, T., Bestley, S., Sallée, J.-B., Fraser, A. D., Sumner, M., Roquet, F., Heerah, K., Picard, B., Guinet, C., Harcourt, R., McMahon, C., Hindell, M. A. and Charrassin, J.-B.: Coastal polynyas: Winter oases for subadult southern elephant seals in East Antarctica, Scientific Reports, 8(1), 3183, doi:10.1038/s41598-018-21388-9, 2018.

Lannuzel, D., Schoemann, V., de Jong, J., Pasquer, B., van der Merwe, P., Masson, F., Tison, J.-L. and Bowie, A.: Distribution of dissolved iron in Antarctic sea ice: Spatial, seasonal, and inter-annual variability, Journal of Geophysical Research: Biogeosciences, 115(G3), doi:10.1029/2009JG001031, 2010.

Li, Y., Ji, R., Jenouvrier, S., Jin, M. and Stroeve, J.: Synchronicity between ice retreat and phytoplankton bloom in circum-Antarctic polynyas, Geophysical Research Letters, 43(5), 2086–2093, doi:10.1002/2016GL067937, 2016.

Lohrenz, S. E., Weidemann, A. D. and Tuel, M.: Phytoplankton spectral absorption as influenced by community size structure and pigment composition, Journal of Plankton Research, 25(1), 35–61, doi:10.1093/plankt/25.1.35, 2003.

Marra, J., Trees, C. C. and O'Reilly, J. E.: Phytoplankton pigment absorption: A strong predictor of primary productivity in the surface ocean, Deep-Sea Research Part I: Oceanographic Research Papers, 54(2), 155–163, doi:10.1016/j.dsr.2006.12.001, 2007.

Mashayek, A., Ferrari, R., Merrifield, S., Ledwell, J. R., St Laurent, L. and Garabato, A. N.: Topographic enhancement of vertical turbulent mixing in the Southern Ocean, Nature Communications, 8, 14197 [online] Available from: https://doi.org/10.1038/ncomms14197, 2017.

van der Merwe, P., Lannuzel, D., Bowie, A. R., Nichols, C. A. M. and Meiners, K. M.: Iron fractionation in pack and fast ice

in East Antarctica: Temporal decoupling between the release of dissolved and particulate iron during spring melt, Deep Sea Research Part II: Topical Studies in Oceanography, 58(9), 1222–1236, doi:https://doi.org/10.1016/j.dsr2.2010.10.036, 2011.

Mitchell, B. G. and Holm-Hansen, O.: Observations of modeling of the Antartic phytoplankton crop in relation to mixing depth, Deep Sea Research Part A, Oceanographic Research Papers, 38(8–9), 981–1007, doi:10.1016/0198-0149(91)90093-U, 1991.

Moore, J. K. and Abbott, M. R.: Phytoplankton chlorophyll distributions and primary production in the Southern Ocean, Journel of Geophysical Research, 105(C12), 28,709-28,722, doi:http://dx.doi.org/10.1029/1999JC000043; doi:10.1029/1999JC000043, 2000.

Morel, A. and Bricaud, A.: Theoretical results concerning light absorption in a discrete medium, and application to specific absorption of phytoplankton, Deep Sea Research Part A, Oceanographic Research Papers, 28(11), 1375–1393, doi:10.1016/0198-0149(81)90039-X, 1981.

Mu, L., Stammerjohn, S. E., Lowry, K. E. and Yager, P. L.: Spatial variability of surface pCO2 and air-sea CO2 flux in the Amundsen Sea Polynya, Antarctica, Elementa: Science of the Anthropocene, 2, 000036, doi:10.12952/journal.elementa.000036, 2014.

Muench, R. D., Morison, J. H., Padman, L., Martinson, D., Schlosser, P., Huber, B. and Hohmann, R.: Maud Rise revisited, Journal of Geophysical Research, 106(C2), 2423, doi:10.1029/2000JC000531, 2001.

Park, J., Oh, I. S., Kim, H. C. and Yoo, S.: Variability of SeaWiFs chlorophyll-a in the southwest Atlantic sector of the Southern Ocean: Strong topographic effects and weak seasonality, Deep-Sea Research Part I: Oceanographic Research Papers, 57(4), 604–620, doi:10.1016/j.dsr.2010.01.004, 2010.

Peck, L. S., Barnes, D. K. A., Cook, A. J., Fleming, A. H. and Clarke, A.: Negative feedback in the cold: Ice retreat produces new carbon sinks in Antarctica, Global Change Biology, 16(9), 2614–2623, doi:10.1111/j.1365-2486.2009.02071.x, 2010.

Planquette, H., Sherrell, R. M., Stammerjohn, S. and Field, M. P.: Particulate iron delivery to the water column of the Amundsen Sea, Antarctica, Marine Chemistry, 153, 15–30, doi:https://doi.org/10.1016/j.marchem.2013.04.006, 2013.

Pond, S., and P. G. L.: Introductory Dynamical Oceanography, 2nd Editio., Butterworh- Heinemann Ltd., Oxford UK., 1983.

Pritchard, H. D., Arthern, R. J., Vaughan, D. G. and Edwards, L. A.: Extensive dynamic thinning on the margins of the Greenland and Antarctic ice sheets, Nature, 461, 971 [online] Available from: https://doi.org/10.1038/nature08471, 2009.

Raiswell, R., Benning, L. G., Tranter, M. and Tulaczyk, S.: Bioavailable iron in the Southern Ocean: the significance of the iceberg conveyor belt., Geochemical transactions, 9, 7, doi:10.1186/1467-4866-9-7, 2008.

Reynolds, R. W. and Smith, T. M.: Improved global sea surface temperature analyses using optimum interpolation, Journal of Climate, 7(6), 929–948, doi:10.1175/1520-0442(1994)007<0929:IGSSTA>2.0.CO;2, 1994.

Roden, G. I.: Effect of Seamounts and Seamount Chains on Ocean Circulation and Thermohaline Structure, in Seamounts, Islands, and Atolls, pp. 335–354, American Geophysical Union (AGU)., 2013.

Rosso, I., Hogg, A. M., Strutton, P. G., Kiss, A. E., Matear, R., Klocker, A. and van Sebille, E.: Vertical transport in the ocean due to sub-mesoscale structures: Impacts in the Kerguelen region, Ocean Modelling, 80, 10–23, doi:https://doi.org/10.1016/j.ocemod.2014.05.001, 2014.

Schofield, O., Miles, T., Alderkamp, A. C., Lee, S. H., Haskins, C., Rogalsky, E., Sipler, R., Sherrell, R. and Yager, P. L.: In situ phytoplankton distributions in the Amundsen Sea Polynya measured by autonomous gliders , Elementa , 3, doi:https://doi.org/10.12952/journal.elementa.000073, 2015.

Selph, K. E., Landry, M. R., Allen, C. B., Calbet, A., Christensen, S. and Bidigare, R. R.: Microbial community composition and growth dynamics in the Antarctic Polar Front and seasonal ice zone during late spring 1997, Deep Sea Research Part II: Topical Studies in Oceanography, 48(19), 4059–4080, doi:https://doi.org/10.1016/S0967-0645(01)00077-7, 2001.

Shadwick, E. H., Tilbrook, B. and Currie, K. I.: Late-summer biogeochemistry in the Mertz Polynya: East Antarctica, Journal of Geophysical Research: Oceans, 122(9), 7380–7394, doi:10.1002/2017JC013015, 2017.

de Steur, L., Holland, D. M., Muench, R. D. and McPhee, M. G.: The warm-water "Halo" around Maud Rise: Properties, dynamics and Impact, Deep-Sea Research Part I: Oceanographic Research Papers, 54(6), 871–896, doi:10.1016/j.dsr.2007.03.009, 2007.

Stirling, I.: The importance of polynas, ice edges, and leads to marine mammals and birds., Journal of Marine Systems, 10(1–4), 9–21, doi:Doi 10.1016/S0924-7963(96)00054-1, 1997.

Strass, V. H., Garabato, A. C. N., Pollard, R. T., Fischer, H. I., Hense, I., Allen, J. T., Read, J. F., Leach, H. and Smetacek, V.: Mesoscale frontal dynamics: shaping the environment of primary production in the Antarctic Circumpolar Current, Deep Sea Research Part II: Topical Studies in Oceanography, 49(18), 3735–3769, doi:https://doi.org/10.1016/S0967-0645(02)00109-1, 2002.

Tagliabue, A., Sallée, J.-B., Bowie, A. R., Lévy, M., Swart, S. and Boyd, P. W.: Surface-water iron supplies in the Southern Ocean sustained by deep winter mixing, Nature Geoscience, 7, 314 [online] Available from: https://doi.org/10.1038/ngeo2101, 2014.

Tamura, T., Ohshima, K. I. and Nihashi, S.: Mapping of sea ice production for Antarctic coastal polynyas, Geophysical Research Letters, 35(7), doi:10.1029/2007GL032903, 2008.

Turner, J., Phillips, T., Marshall, G. J., Hosking, J. S., Pope, J. O., Bracegirdle, T. J. and Deb, P.: Unprecedented springtime retreat of Antarctic sea ice in 2016, Geophysical Research Letters, 44(13), 6868–6875, doi:10.1002/2017GL073656, 2017.

Wagener, T., Guieu, C., Losno, R., Bonnet, S. and Mahowald, N.: Revisiting atmospheric dust export to the Southern Hemisphere ocean: Biogeochemical implications, Global Biogeochemical Cycles, 22(2), doi:10.1029/2007GB002984, 2008.

Wåhlin, A. K., Yuan, X., Björk, G. and Nohr, C.: Inflow of Warm Circumpolar Deep Water in the Central Amundsen Shelf, Journal of Physical Oceanography, 40(6), 1427–1434, doi:10.1175/2010JPO4431.1, 2010.

Weijer, W., Veneziani, M., Stössel, A., Hecht, M. W., Jeffery, N., Jonko, A., Hodos, T. and Wang, H.: Local atmospheric response to an open-ocean polynya in a high-resolution climate model, Journal of Climate, 30(5), 1629–1641, doi:10.1175/JCLI-D-16-0120.1, 2017.

Westberry, T., Behrenfeld, M. J., Siegel, D. A. and Boss, E.: Carbon-based primary productivity modeling with vertically resolved photoacclimation, Global Biogeochemical Cycles, 22(2), 1–18, doi:10.1029/2007GB003078, 2008.

White, M. and Mohn, C.: Review of Physical Processes at Seamounts, Oceanic Seamounts: An Integrated Study, 2002.

Williams, N. L., Juranek, L. W., Feely, R. A., Johnson, K. S., Sarmiento, J. L., Talley, L. D., Dickson, A. G., Gray, A. R., Wanninkhof, R., Russell, J. L., Riser, S. C. and Takeshita, Y.: Calculating surface ocean pCO2 from biogeochemical Argo

floats equipped with pH: An uncertainty analysis, Global Biogeochemical Cycles, 31(3), 591–604, doi:10.1002/2016GB005541, 2017.

Yager, S., Bertilsson, S., Lowry, K., Severmann, P., Schofield, O., Wilson, S., Stammerjohn, S., Moksnes, P.-O., Thatje, S., Riemann, L., van Dijken, G., Garay, L., Abrahamsen, P., Post, A., Ndungo, K., Alderkamp, A.-C., Guerrero, R., Sherrell, R., Randall-Goodwin, E. and Arrigo, K.: ASPIRE: The Amundsen Sea Polynya International Research Expedition, Oceanography, 25(3), 40–53, doi:10.5670/oceanog.2012.73, 2012.

Zanowski, H., Hallberg, R. and Sarmiento, J. L.: Abyssal Ocean Warming and Salinification after Weddell Polynyas in the GFDL CM2G Coupled Climate Model, Journal of Physical Oceanography, 45(11), 2755–2772, doi:10.1175/JPO-D-15-0109.1, 2015.

Supplementary Figures

Text S1 to S8~~6~~

Figures S1 to S8~~6~~

Text S1. (a) We have analyzed monthly sea-ice concentration (SIC) data (September to November 2017) from the passive microwave sensors with spatial resolution of 25 km acquired from the National Snow and Ice Data Center (NSIDC) (Data id-G02135, Version 3, https://nsidc.org/data). The data were generated using the NASA Team algorithm, which converts satellite derived brightness temperatures to gridded SIC (Cavalieri, D. J., C. L. Parkinson, P. Gloersen, 1997). The sea-ice anomaly for different year was computed relative to the climatology covering the period of 1979-2015. Red rectangle shows the anomalous record lowest sea-ice area and extent observed since three successive years from 2016 to 2018 with the maximum melting occurred in 2017. (b) We analyzed monthly mean sea-ice extent data from NSIDC (Data id-G02135, Version 3) indicating loss of sea-ice that started from September 2016 and continued for the year 2017, 2018 and 2019. (c) We used ocean potential temperature data from global marine Argo atlas (http://www.argo.ucsd.edu/Marine_Atlas.html#) that indicated anomalous upper ocean warming of the Southern Ocean from 2016 to 2018. The potential temperature was spatially averaged over the south of 55°S region encircling the Antarctica. The likelihood for the occurrence of the polynya is quite high with a background of anomalous upper ocean warming and sea-ice loss.

Text S2. In order to analyze the Aqua-MODIS derived net primary production (NPP), we have validated three ocean-color based models such as the vertically generalized production model (VGPM), *Eppley*-VGPM, and carbon-based productivity model (CbPM) for selecting the best model for the study region. We evaluated the performance of these models by comparing with the in-situ NPP estimated using ^{13}C tracer during the Indian scientific expedition to the Southern Ocean in 2009. The locations of in-situ NPP observations during the austral summer (February to April 2009) are presented in figure S2a. The in-situ NPP from 11 observations range from about 85.04 to 923.83 mg C m^{-2} day^{-1}. The detail method of ^{13}C measurement was documented in the previous work (Gandhi et al., 2012). The model based NPP values were available in weekly time scale with a spatial resolution of ~4 km (https://www.science.oregonstate.edu/ocean.productivity). The pixel values from the models were extracted around each in-situ observation to generate the matchups for the validation strategy, a method adopted by several authors (Babula Jena, 2017; R. Johnson et al., 2013). The comparative statistical analysis suggested that the scatters were much better in the case of *Eppley*-VGPM estimated NPP (Fig. S2c) than those in the case of VGPM (Fig. S2b) and CbPM (Fig. S2d).

Text S3. We analysed eddy-resolving model data available from Copernicus Marine Environment Monitoring Service (CMEMS) global analysis and forecast (http://marine.copernicus.eu/services-portfolio/access-to-products/, GLOBAL_ANALYSIS_FORECAST_PHY_001_024). The detailed methodology of product generation, and quality control

approaches for this data is given online at http://cmems-resources.cls.fr/documents/QUID/CMEMS-GLO-QUID-001-024.pdf. Figure S3 shows depth-latitude cross section of ocean temperature along 4.7°E during (a) September, (b) October, and (c) November 2017.

~~***Text S4.*** *Hydrographic Potential temperature profiles from an Argo float (ID-5904468) located at the edge of the Maud Rise polynya were analyzed for August-December 2017. The Argo data are being generated from the Southern Ocean Carbon and Climate Observations and Modeling (SOCCOM) Project funded by the National Science Foundation, Division of Polar Programs (NSF PLR -1425989), supplemented by NASA, and by the International Argo Program and the NOAA programs. The data are available at https://www.mbari.org/science/. Figure S4 provided evidence on the upliftment of thermocline during the formation of polynya.~~

Text S4~~5~~. Hydrographic profiles (potential temperature, salinity, density, mixed layer and water column stability) from an Argo float (ID-5904468) on the Maud Rise starting from 2015 through 2019. The profiles indicated mixed layer warming ~~on~~ during spring 2016 and 2017. The upwelling of high saline and warm water into the mixed layer facilitated the sea-ice melting. The melting of sea-ice leads to the development of shallow mixed layer due to the accumulation of freshwater in the upper ocean. Therefore, we observed lower values of salinity in the mixed layer with increased stability of the water column. The development of shallow mixed layer improved the light availability in the upper ocean and the condition is favourable for the growth of phytoplankton. The Argo data are being generated from the Southern Ocean Carbon and Climate Observations and Modeling (SOCCOM) Project funded by the National Science Foundation, Division of Polar Programs (NSF PLR -1425989), supplemented by NASA, and by the International Argo Program and the NOAA programs. The data are available at https://www.mbari.org/science/.

Text S5. Monthly averaged values of photosynthetically available radiation were acquired from Aqua-MODIS during the appearance of polynya in October and November 2017. The bloom was appeared in October-November 2017 under the influence of improved light condition up to 36.1 and 61.9 Einstein m-2 day-1, respectively for October and November.

Text S6. Monthly anomalies of shortwave radiation for September-November 2017 was computed relative to a 38-year climatology (1979-2016). The regions within grey polylines shows the record level shortwave radiation in 2017 that lies outside of shortwave radiation values from 1979 to 2016. The monthly incident shortwave radiation was acquired from the European Center for Medium-Range Weather Forecast (ECMWF) (grid resolution of 0.25°) during January 1979-December 2017.

Text S7~~5~~. Argo data were utilized to find the linkage between the observed bloom and the ocean pCO_2 condition. The data are available at https://www.mbari.org/science/. Low pCO_2 values that reached as low as 372.8 µatm (Figure 4d)

Formatted: Font: Italic

Formatted: Font: Not Bold

Formatted: Font: 10 pt

Formatted: Font: (Default) +Headings (Times New Roman), Bold

Formatted: Font color: Auto

corresponding to the bloom occurrence during October-November 2017 (Figure 4a). The pCO_2 values declined during the occurrence of bloom in comparison with the period of no bloom condition in August-September 2017, 2015 and 2016 (Figure 4). The coefficient of correlation (r) between the pCO_2 and chl-*a* was -0.56 ($p < 0.01$) during August-September 2017 (Figure S4a). The relationship improved ($r = -0.82$, $p < 0.01$) and the spatial pattern closely matched together during the bloom condition in October-November 2017 (Figures S4b and 4a-d). The best relationship observed between the pCO_2 and chl-*a* when the data was log transformed ($r = -0.94$, $p < 0.01$).

Text S8~~6~~. Daily sea-ice concentration (SIC) data from the Special Sensor Microwave Imager Sounder (SSMIS) with spatial resolution of 25 km acquired from the National Snow and Ice Data Center (NSIDC) (Data id-G02135, Version 3, https://nsidc.org/data). The data were generated using the NASA Team algorithm, which converts satellite derived brightness temperatures to gridded SIC (Cavalieri, D. J., C. L. Parkinson, P. Gloersen, 1997). The accuracy SIC is within 5% of the actual SIC in winter, and within 15% in summer when the melt ponds are present on the sea ice (Fetterer et al., 2016). Several algorithms are available for converting the microwave brightness temperatures of different frequencies to SIC. In higher SIC and thickness (more than 20 cm), the achieved accuracy is found to be better. The detail information about the sensor description, sea-ice processing methods, synoptic coverage, resolution, projection, validation, and the limitations of sea-ice retrieval from passive microwave sensors are given in an earlier article (Fetterer et al., 2016). Figure ~~S6~~ S8 shows the reappearance of the Weddell Sea (red rectangle) and Maud Rise (black rectangle) polynyas starting ~~Weddell Sea and Maud Rise polynya (within the rectangle)~~ from 23 November 2018 to 12 December 2018. The polynya disappeared in 13 December 2018.

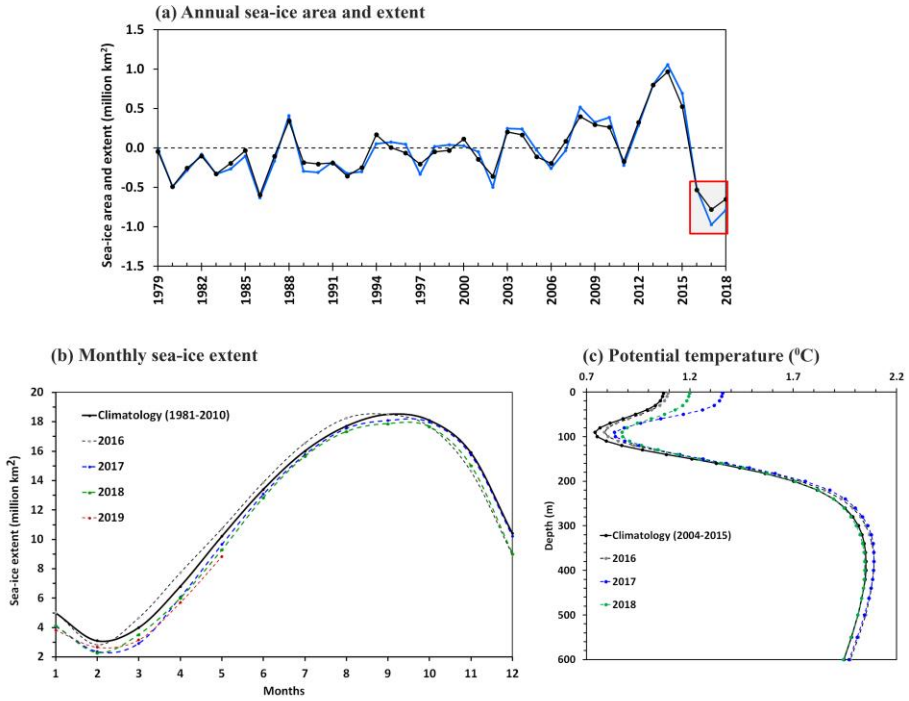

90 **Fig. S1** (a) Inter-annual variability of Antarctic sea-ice area (black) and extent (blue) anomaly relative to the climatology (1979-2015), as analyzed from satellite observations of passive microwave sensors. Red rectangle shows the anomalous record lowest sea-ice area and extent observed since three successive years from 2016 to 2018 with the maximum melting occurred in 2017. (b) Monthly mean sea-ice extent data indicated loss of sea-ice that started from September 2016 and continued for the year 2017, 2018 and 2019. (c) Argo based ocean potential temperature data (2004-2018) indicated
95 anomalous upper ocean warming of the Southern Ocean from 2016 to 2018. The potential temperature was spatially averaged over the south of 55°S region encircling the Antarctica. The likelihood for the occurrence of the polynya is quite high with a background of anomalous upper ocean warming and sea-ice loss.

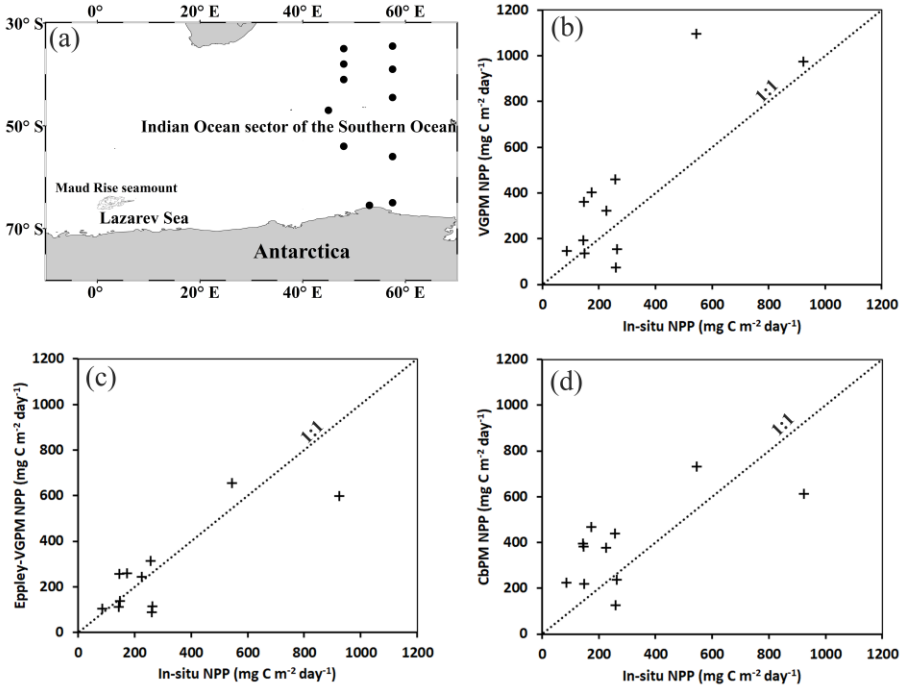

Fig. S2 (a) Filled circles showing the locations of in-situ net primary production (NPP) from ^{13}C tracer during the Indian scientific expedition to the Southern Ocean (February to April 2009). Scatter plots between in-situ NPP and (b) VGPM, (c) *Eppley*-VGPM, (d) CbPM NPP estimations. In-situ measurements had significant positive relationship with the NPP values derived from *Eppley*-VGPM (r = 0.82, p = 0.001), VGPM (r = 0.82, p = 0.001) and CbPM (r = 0.66, p = 0.026). However, the NPP values from VGPM and CbPM indicating significant overestimations. NPP- net primary production, CbPM- carbon based productivity model, VGPM- vertically generalized production model.

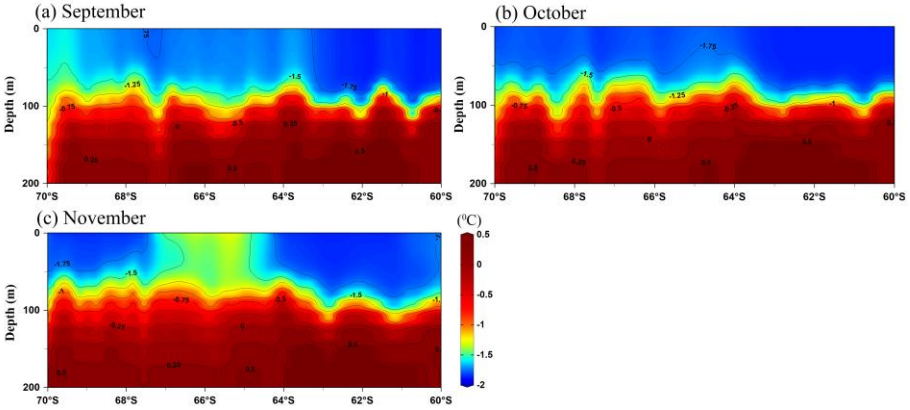

Fig. S3 Depth-Latitude cross section of ocean temperature (along 4.7°E) during (a) September, (b) October, and (c) November 2017, using a high-resolution (1/12°) eddy-resolving model from the Copernicus Marine Environment Monitoring Service (CMEMS).

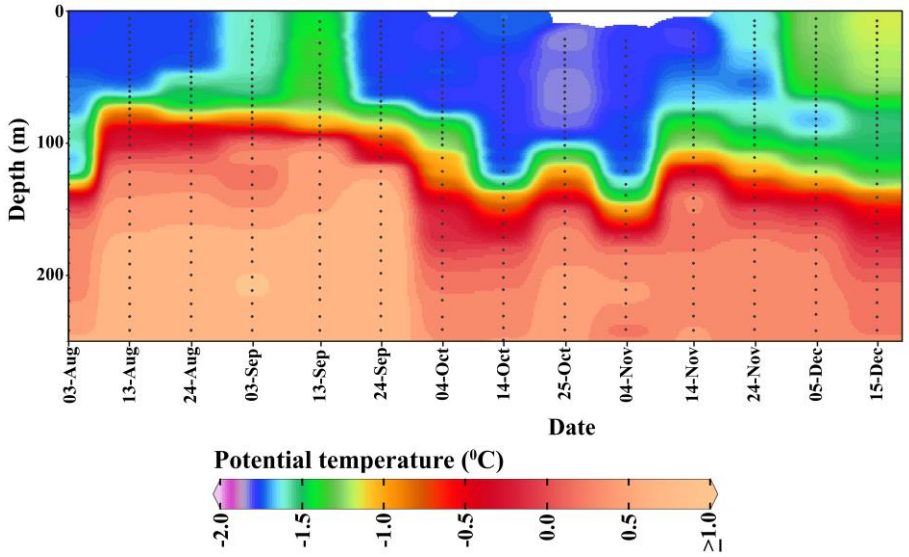

~~**Fig. S4** Potential temperature pProfiles from an Argo float (ID-5904468) located at the edge of the Maud Rise polynya during August-December 2017, provided evidence on the upliftment of thermocline.~~

Formatted: Font: Not Bold

115

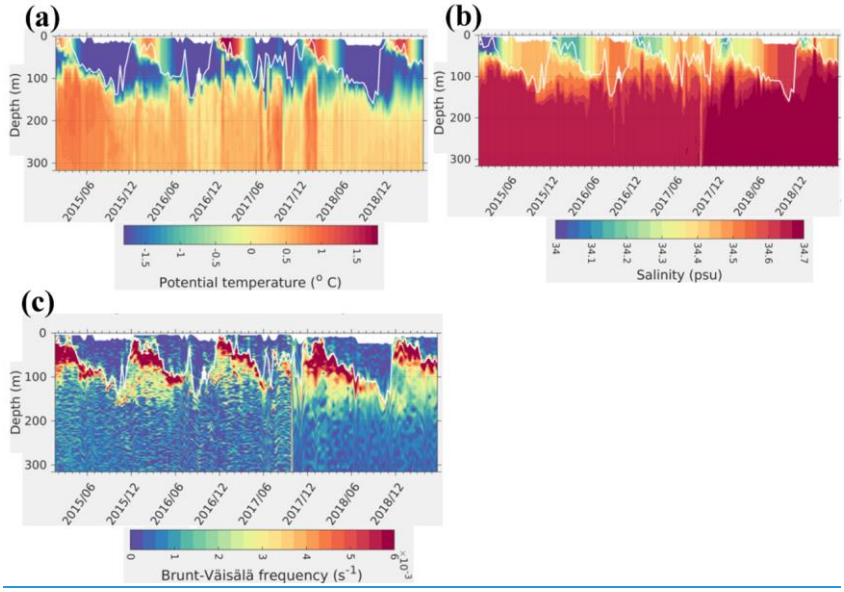

Fig. S45 ARGO float (id-5904468) on the Maud Rise showing (a) potential temperature, (b) salinity, and (c) static stability of the upper ocean. The profiles indicated mixed layer warming on the Maud Rise during spring 2016 and 2017. White solid line in each panel shows the variability of mixed layer depth.

Formatted: Font: Bold

Formatted: Font: Bold

Formatted: Font: (Default) Times New Roman, Not Bold

120

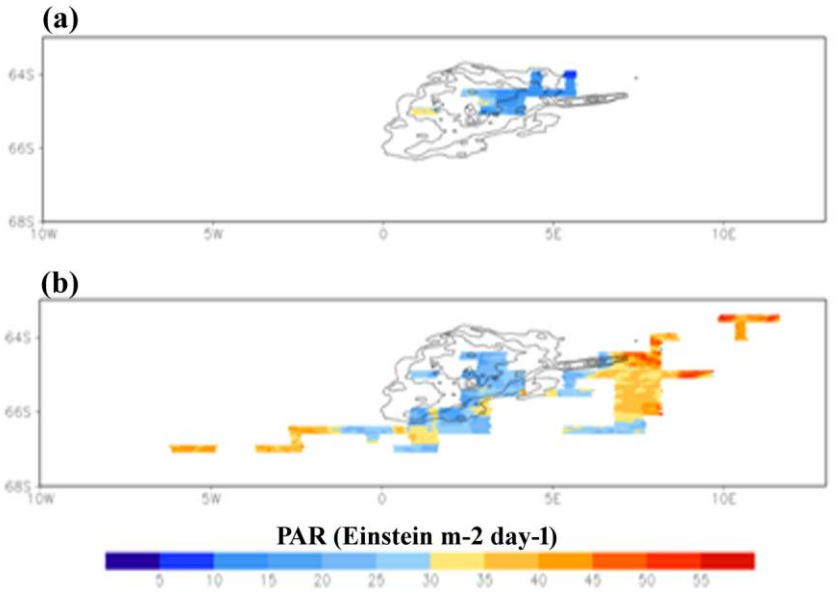

Fig. S5~~6~~ Monthly averaged values of Aqua-MODIS photosynthetically available radiation during the appearance of polynya in (a) October and (b) November 2017.

Formatted: Font: Bold

Formatted: Font: Bold

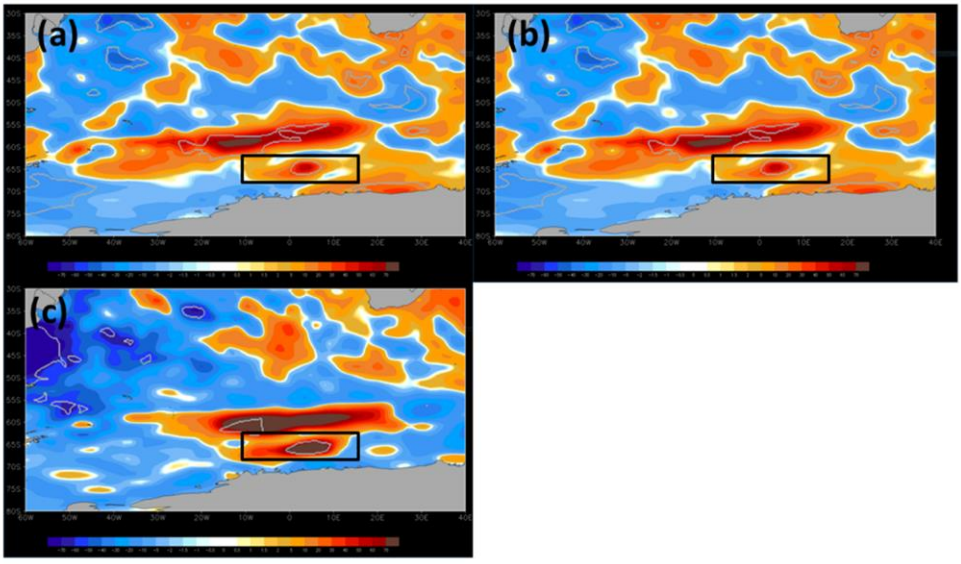

Fig. S6 Monthly anomalies of incident shortwave radiation for (a) September, (b) October, and (c) November 2017 in the Maud Rise polynya (black rectangles). The anomalies were computed relative to a 38-year climatology (1979-2016). The regions within grey polylines shows the record level shortwave radiation in 2017 that lies outside of shortwave radiation values from 1979 to 2016. The data were acquired from the European Center for Medium-Range Weather Forecast (ECMWF) at a grid resolution of 0.25°.

Formatted: Font: Not Bold

Formatted: Font: Not Bold

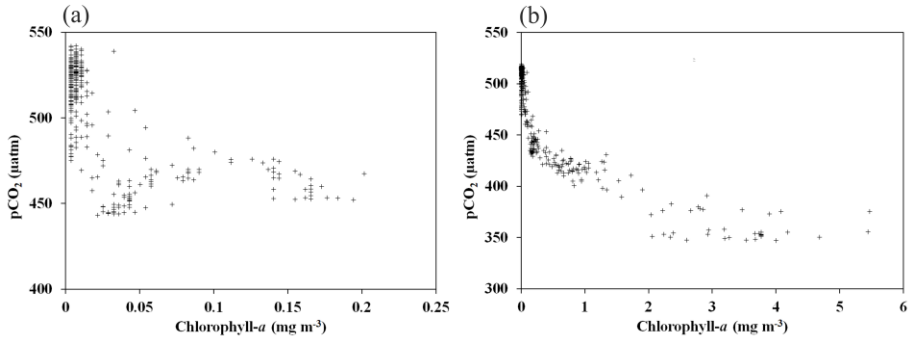

Fig. S7~~5~~ Argo data were utilized to find the relationship between the chlorophyll-*a* and the oceanic pCO_2 condition. (a) The coefficient of correlation (r) between the pCO_2 and chl-*a* was found to be -0.56 ($p < 0.01$) during August-September 2017. (b) The relationship improved (r = -0.82, $p < 0.01$) during the bloom condition in October-November 2017. The best relationship observed between the pCO_2 and chl-*a* when the data was log transformed (r = -0.94, $p < 0.01$).

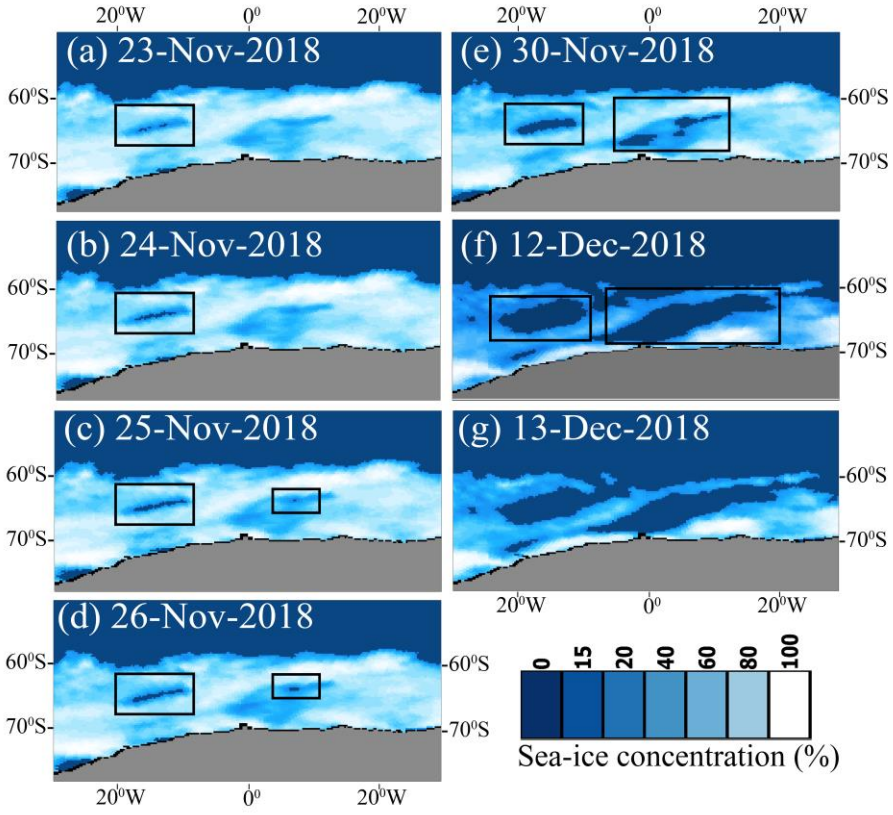
20⁰W
0⁰
20⁰W
(a) 23-Nov-2018
(b) 24-Nov-2018
(c) 25-Nov-2018
(d) 26-Nov-2018
(e) 30-Nov-2018
(f) 12-Dec-2018
(g) 13-Dec-2018
60⁰S
70⁰S
0
15
20
40
60
80
100
Sea-ice concentration (%)

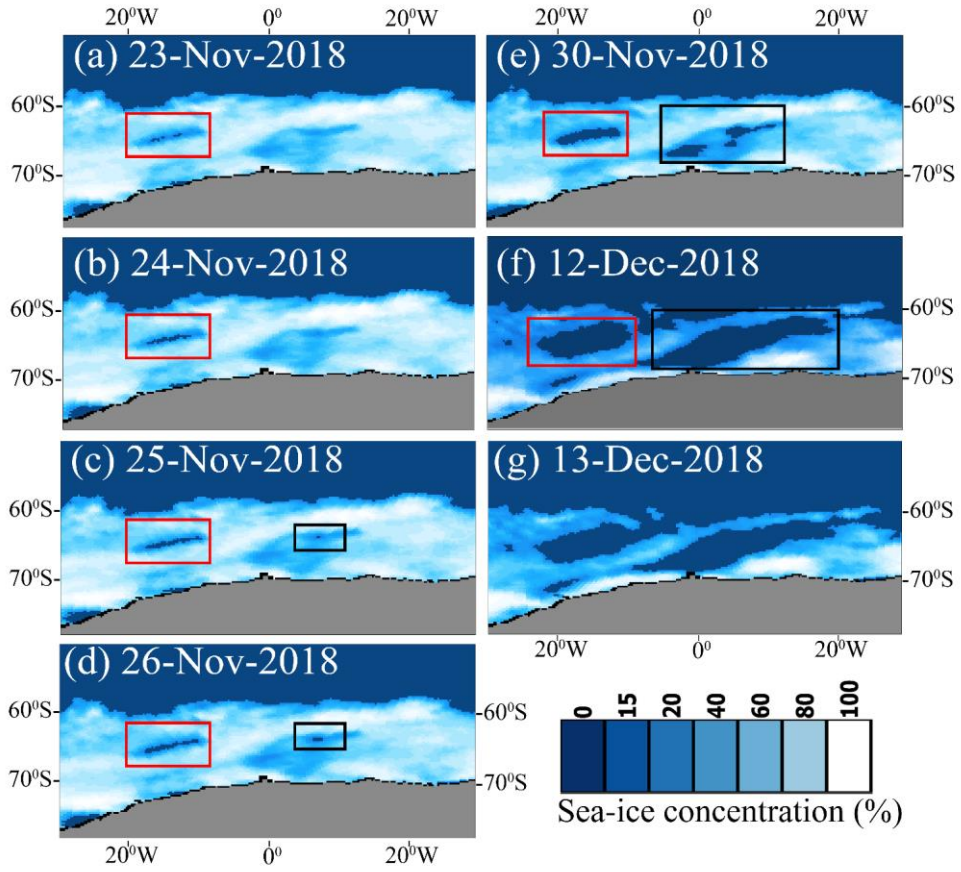

Fig. S~~6~~8 The Special Sensor Microwave Imager Sounder (SSMIS) shows the reappearance of the Weddell Sea (red rectangle) and Maud Rise ~~polynya (within the~~black rectangle) polynyas starting from 23 November 2018 to 12 December 2018. The polynya disappeared in 13 December 2018.